Prioritizing Agricultural Flood Mitigation: A GeoAI-Driven Assessment of Susceptibility, Crop Exposure, and Socioeconomic Vulnerability

Mirza Md Tasnim Mukarram[a,b], Mirza Waleed[c*], Quazi Umme Rukiya[a], Marc Linderman[a], Ibrahim Demir[d,e]

[a] School of Earth, Environment and Sustainability, University of Iowa, Iowa City, IA 52242, USA

[b] Department of Computer Science, University of Iowa, Iowa City, IA 52242, USA

[c] Department of Geography, Hong Kong Baptist University, Hong Kong Special Administration Region of China

[d] River-Coastal Science and Engineering, Tulane University, New Orleans, LA, USA

[e] ByWater Institute, Tulane University, New Orleans, LA, USA

*** Corresponding Author Email (WALEED M.):** waleedgeo@outlook.com

Corresponding Author Address: Office AAB1228, Academic and Administration Building, Hong Kong Baptist University, Hong Kong Special Administration Region of China

Abstract

Flooding is a recurrent hazard across the U.S. Midwest, yet frameworks integrating flood hazard, agricultural exposure, and socioeconomic vulnerability at the county scale remain limited. This study presents a GeoAI-driven agricultural flood risk assessment for all 99 counties in Iowa, combining machine learning-derived flood susceptibility with crop-specific economic exposure and socioeconomic vulnerability within a hazard–exposure–vulnerability (HEV) framework. Using ten 30m resolution conditioning factors, a LightGBM model was optimized and interpreted via SHAP, identifying elevation, rainfall frequency, and river proximity as dominant susceptibility drivers (ROC-AUC = 0.95, F1-score = 0.90). This susceptibility surface—classifying 13.3% of Iowa as high and very high susceptibility—was integrated with 2022 USDA Census data representing $17.6 billion in combined corn and soybean value, alongside a five-indicator socioeconomic vulnerability index. The integrated HEV analysis identified Black Hawk County as possessing the highest compound agricultural risk, while Monona County recorded the highest scenario-based annualized loss. Statewide, annualized agricultural flood losses are estimated at $527.7 million, equivalent to 3.04% of gross crop revenue. Furthermore, spatial hotspot analysis revealed a persistent risk cluster within the Cedar River watershed, allowing for the classification of 48 counties as Priority 1 intervention areas. By translating technical susceptibility mapping into actionable economic and spatial risk metrics, this scalable framework provides critical decision-support for agricultural disaster risk reduction, targeted climate adaptation, and resource allocation in intensive farming regions.

Keywords: Agricultural flood risk; Hazard–exposure–vulnerability; Socioeconomic vulnerability; Crop exposure; Disaster risk reduction; County-scale risk assessment

1. Introduction

Flooding is a recurring natural hazard with far-reaching impacts on society, and losses from storms and floods have steadily increased over the past decades, with losses in 2017 costing the global economy over $140 billion USD and the subsequent four out of five years from 2018 through 2023 each exceeding $100 billion USD annually [1]. Over 2.2 billion people worldwide are currently exposed to flooding, with global flood risk projected to grow from 1.81 billion people today to 2.3 billion by 2050 [2,3]. Floods generate more than $40 billion in economic losses each year, and climate-related disasters broadly are projected to cost over $300 billion per year in direct asset losses, rising to $520 billion when indirect costs are included [2,4]. In the United States, flood damage averaged USD 7.96 billion per year from 1985 to 2014, more than $39 billion in flood insurance claims were paid between 1984 and 2020, and nearly 41 million people live within the 100-year flood zone [5,6]. Flooding accounts for over 45% of all presidential disaster declarations nationally [7]. Approximately 19 million Americans live in areas where high flood exposure and high social vulnerability converge, predominantly in rural communities [8].

Agricultural losses represent a consistently under quantified component of total flood damage. Damage to the agricultural sector is routinely undercounted in post-event assessments, not because the true impact is smaller, but because spatially resolved crop-specific flood damage models have historically been absent from the literature [9]. In Vietnam's Vu Gia-Thu Bon basin, annual average agricultural flood risk reached 6% of total production value, with indirect and intangible losses accounting for 62% of that total, a share consistently excluded from conventional damage frameworks [10]. In Florida, the agricultural value at risk from Hurricane Irma flooding reached $940 million across vegetable crops statewide [11]. In Pakistan, the 2010 flood destroyed 2 million hectares of cropland and generated $10 billion in cumulative economic losses, with subsequent research confirming that farm size, income fragility, and land tenure are primary structural drivers of agricultural flood vulnerability [12,13]. Such integrated frameworks that simultaneously quantify flood hazard, crop-specific economic exposure, and socioeconomic vulnerability remain largely absent at the county scale for major U.S. agricultural regions.

Iowa is one of the most severely flood-exposed agricultural landscapes in the United States. Agribusiness covers approximately 85% of the state's land area, and Iowa's corn-soybean system generates annual gross revenues exceeding $17 billion [14]. Presidential disaster declarations have been issued almost every year in Iowa for the past three decades [2]. Catastrophic events struck in 1993, 2008, 2014, 2016, and 2019, with the 2008 Cedar River flood displacing nearly 24,000 Cedar Rapids residents and the 2019 floods causing an estimated $1.6 billion in statewide damage [15]. Another study estimated over $230 million in average annualized agricultural flood losses using static FEMA floodplain extents and found nearly half a million acres of cropland within the 2-year flood zone [14], but that study lacked a continuous ML-derived hazard layer, county-scale crop-specific loss decomposition, and socioeconomic vulnerability integration. A very recent research showed that during flooding, displaced population, impacted properties, and disrupted road lengths across Iowa counties can reach 46%, 41%, and 40% respectively, with 25% of counties qualifying as very high exposure

areas, yet that framework was limited to the built environment and identified agricultural economic loss quantification as a key unresolved gap [16]. A county-scale framework that combines a data-driven hazard layer, crop-specific exposure, and socioeconomic vulnerability into a unified loss model has not been established for Iowa.

Machine learning and GeoAI have emerged as robust, scalable alternatives to static and physics-based flood models across diverse geographic settings. Recent research demonstrates that ML architectures, particularly gradient boosting models and hybrid ensembles, achieve exceptional predictive accuracy, consistently outperforming conventional bivariate statistical models and producing highly defensible flood risk zoning. Furthermore, integrating these ML-derived hazard surfaces with vulnerability layers via a multiplicative framework has proven to be a superior approach for mapping compound risk compared to traditional methods [9, 17, 18, 19]. Waleed & Sajjad (2025) benchmarked 14 ML models and identified LightGBM as the top performer for accuracy-focused flood susceptibility mapping, while their national-scale GeoAI framework at 30-meter resolution across Pakistan found that 29% of total land area falls under critical susceptibility with 95 million people exposed [20]. The IPCC-aligned H x E x V multiplicative framework has been validated from India to the Ganges Delta, consistently identifying compound risk concentrations that single-dimension analyses cannot detect [21,22]. SHAP analysis addresses the interpretability gap of gradient boosting models by attributing individual predictions to physically meaningful drivers [23]. Despite this methodological progress, the combination of an ML-derived hazard surface, crop-specific exposure, and socioeconomic vulnerability within a unified county-scale agricultural flood loss pipeline has not been demonstrated for any major U.S. agricultural region.

Against this background, the present study develops an integrated agricultural flood risk assessment for Iowa state that combines flood hazard, crop-specific exposure, and socioeconomic vulnerability within a unified hazard–exposure–vulnerability framework. Rather than treating flood susceptibility as an end-product, the study uses it as one component of a broader risk assessment designed to identify where agricultural systems are most exposed to flood impacts and where intervention needs are greatest. By linking spatial flood patterns with county-level crop value, farm structural conditions, and comparative loss estimates, the framework provides a more policy-relevant understanding of agricultural flood risk across Iowa's 99 counties. The study further supports disaster risk reduction by identifying spatial hotspots and priority counties where adaptation planning, targeted mitigation, and agricultural risk management measures may be most urgently required. In this way, the paper contributes a scalable and transferable approach for strengthening agricultural resilience in Iowa and other intensively farmed flood-prone regions.

2. Methodology

The methodological framework in this study combines geospatial data processing, machine learning-based flood susceptibility modeling, and an IPCC-aligned HEV agricultural risk assessment [24] to quantify county-level agricultural flood risk and expected economic loss across Iowa's 99 counties. All spatial datasets were standardized to NAD83/UTM Zone 15N at

30 m resolution. The complete methodological workflow is illustrated in Figure 1 and details are provided afterwards.

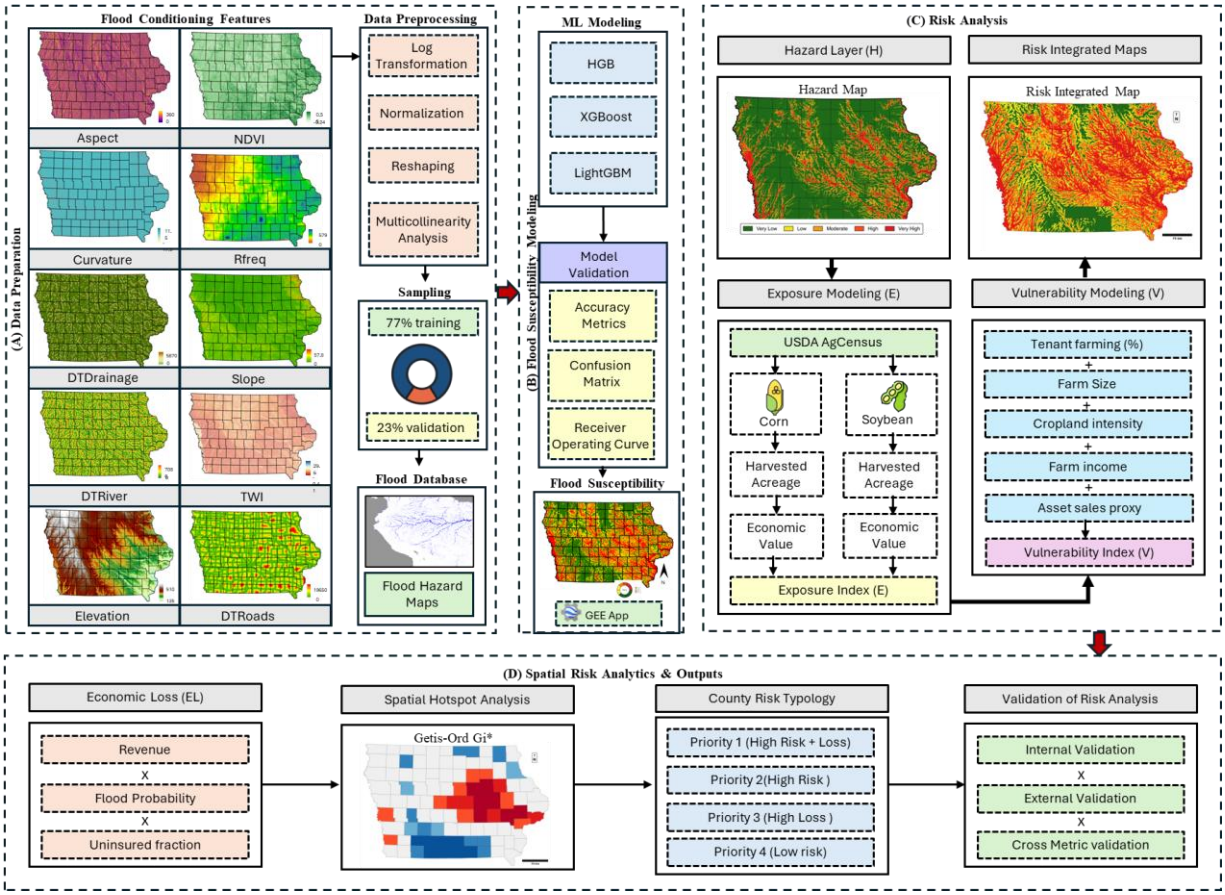

Figure 1 Methodology flowchart showing the overall framework for this study. (A,B) ML-based flood susceptibility modeling framework from ten flood conditioning features through gradient boosting model benchmarking (XGBoost, LightGBM, HistGBM), SHAP explainability, and GEE web application deployment; (C) H × E × V agricultural risk integration framework from hazard, exposure, and vulnerability inputs through multiplicative risk integration (D) economic loss estimation, Getis-Ord Gi* hotspot analysis, and county risk typology.

2.1. Study Area

Iowa is located in the U.S. Midwest, covering approximately 145,746 km² across 99 counties (Figure 2). The state is bounded by the Mississippi River to the east and the Missouri River to the west, with the Cedar, Des Moines, and Iowa Rivers constituting the primary interior drainage network, connecting major urban centers to the broader agricultural plains [16]. The terrain is characteristically flat to gently sloping, a product of Late Pleistocene glaciation, with low natural water storage capacity that produces rapid runoff responses under saturated conditions. These physical predispositions have been compounded by intensive anthropogenic modification: widespread subsurface tile drainage installation combined with the reduction of mature vegetation has decreased soil infiltration capacity and accelerated peak flows into downstream communities [14,25]. Approximately 87% of the state's land cover is agricultural or urban, with nearly 13 million acres under corn and 9 million acres under soybeans, making Iowa a cornerstone of U.S. food production. The state sustains a population of approximately 3.1 to 3.25 million, with major urban centers including Des Moines, Cedar Rapids, Iowa City, Waterloo, and Cedar Falls situated directly adjacent to active floodplains [16,26]. Cedar

Rapids, the second-largest city with a population of approximately 137,710, occupies low-elevation terrain between 213 and 270 m and has experienced repeated catastrophic inundation [2]. Statewide, approximately 100,000 residents live within the 100-year floodplain and an estimated 390,000 properties are classified as flood-exposed [26]. The 2008 flood event alone displaced over 40,000 residents statewide and caused approximately $10 billion in damages, while the 2019 Missouri River and basin floods generated approximately $1.6 billion in additional losses [15,26]. This spatial convergence of hydrologically active corridors, intensive agricultural land use, dense urban settlement, and structurally vulnerable populations positions Iowa as the study domain for the GeoAI-driven HEV risk integration framework applied here.

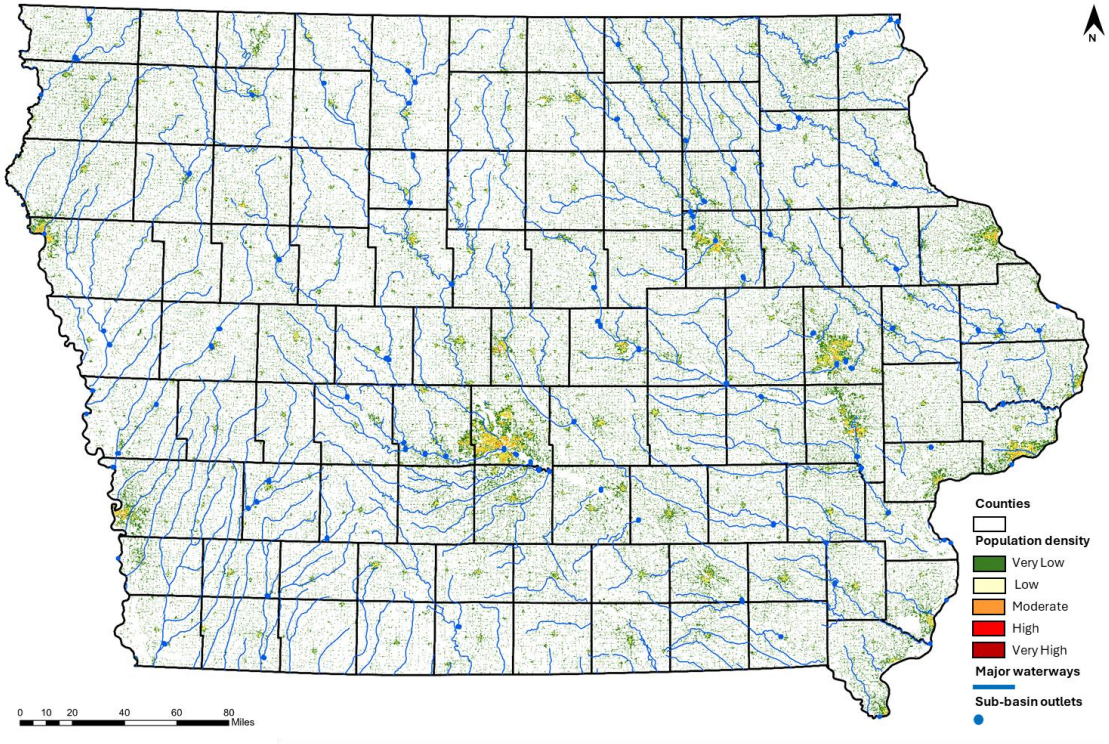

Figure 2 Study area map of Iowa showing 99 county boundaries, major river systems (Missouri, Mississippi, Cedar, Des Moines, and Iowa Rivers), and sub-basin outlet network.

2.2. Data Collection

All datasets used in this study were sourced from openly accessible federal and global repositories, ensuring full reproducibility and transferability of the framework to other data-scarce agricultural regions. Flood conditioning features (FCFs), agricultural exposure indicators, and socioeconomic vulnerability inputs were compiled from publicly available geospatial and census platforms, as detailed below. Based on recent studies [2,3], ten FCFs were selected to represent the topographic, hydrological, climatic, and anthropogenic drivers of flood susceptibility (Table 1, Figure 3). Topographic variables, including elevation, slope, aspect, curvature, and TWI, were derived from the FABDEM [27], a 30 m bare-earth global digital elevation model. The Topographic Wetness Index (TWI) was computed using Equation (1).

$$\mathrm{TWI} = \ln\left(\frac{\alpha}{\tan\beta}\right) \tag{1}$$

where α is the upslope contributing area per unit contour width (m^2/m) and β is the local slope angle in degrees. NDVI was derived from Landsat 8 OLI imagery using Equation (2).

$$\mathrm{NDVI} = \frac{\rho_{\mathrm{NIR}} - \rho_{\mathrm{Red}}}{\rho_{\mathrm{NIR}} + \rho_{\mathrm{Red}}} \quad (2)$$

where ρ_{NIR} and ρ_{Red} are surface reflectance values in the near-infrared and red bands, respectively. Hydrological proximity variables were computed using HydroSHEDS vectors [28] and OpenStreetMap road networks [29]. Rainfall frequency was derived from CHIRPS v2 [30] over 2010–2024. Binary flood inundation training labels were sourced from the WRI Aqueduct Global Flood Analyzer [31]. All ten features satisfied multicollinearity screening criteria (VIF < 10; inter-feature Pearson $r < 0.75$).

Agricultural exposure and vulnerability data were sourced from the USDA National Agricultural Statistics Service (NASS) Census of Agriculture 2022, the most recent quinquennial census publicly available at the time of analysis (released February 2024), accessed via the NASS QuickStats API [32]. The 2022 Census provides the only publicly available county-level dataset containing all five required vulnerability indicators simultaneously and ensures temporal alignment with the flood susceptibility model conditioning features and USDA RMA 2022 records used for external validation. Crop prices reflect 2022 Iowa marketing-year averages: corn at $4.50/bu and soybeans at $11.50/bu.

Table 1 Details of 10 flood conditioning features used in this study

Feature	Description	Source	Category
Elevation	Bare-earth surface; primary inundation depth driver	FABDEM 30 m	Topographic
Slope	Rate of elevation change; controls flow velocity	FABDEM 30 m	Topographic
Aspect	Slope orientation; drainage asymmetry	FABDEM 30 m	Topographic
Curvature	Concavity/convexity; flow convergence zones	FABDEM 30 m	Topographic
TWI	ln(α/tan β); terrain soil saturation proxy	FABDEM 30 m	Hydrological
NDVI	(NIR−Red)/(NIR+Red); land cover/runoff proxy	Landsat 8 OLI	Land cover
Rainfall Freq.	Days/yr >10 mm; precipitation recurrence intensity	CHIRPS v2 2010–2024	Climatic
DTRiver	Distance to nearest river; flood proximity	HydroSHEDS	Hydrological
DTDrainage	Distance to drainage network; catchment connectivity	HydroSHEDS	Hydrological
DTRoads	Distance to road network; infrastructure exposure	OpenStreetMap	Anthropogenic

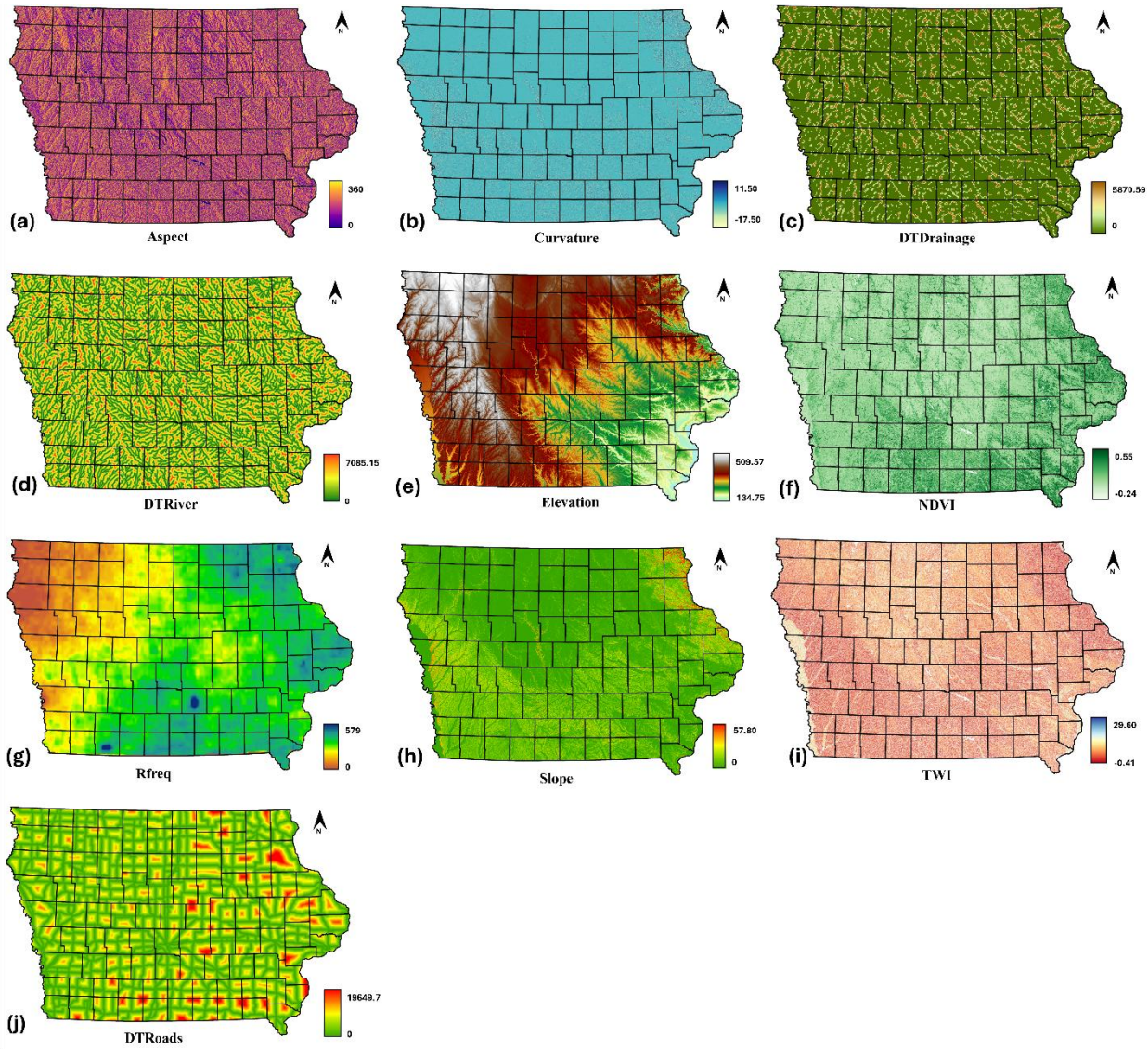

Figure 3 Spatial visualization of Flood conditioning feature for Iowa state at 30m. (a) aspect, (b) curvature, (c) distance to drainage, (d) distance to river, (e) elevation (FABDEM 30 m), (f) NDVI (Landsat 8 OLI), (g) rainfall frequency (CHIRPS v2, 2010–2024), (h) slope, (i) TWI, (j) distance to roads

2.3. Data Preprocessing

Each FCF was log-transformed as $\ln(\delta + \gamma)$ to reduce the influence of extreme values and stabilize variance. Features were then rescaled to [0,1] using directional min-max normalization. Features positively associated with flood susceptibility were normalized using Equation (3).

$$\hat{x} = \frac{\delta - \delta_{\min}}{\delta_{\max} - \delta_{\min}} \tag{3}$$

Where $\hat{x}$ represents normalized feature, and δ indicates raw feature value. Features inversely related to flood susceptibility (elevation and NDVI) were normalized using Equation (4).

$$\hat{x} = \frac{\delta_{\max} - \delta}{\delta_{\max} - \delta_{\min}} \tag{4}$$

Multicollinearity among the preprocessed features was then evaluated using Pearson correlation matrices (Figure 4) and variance inflation factors; all ten FCFs satisfied the established independence criteria, confirming their suitability as model inputs.

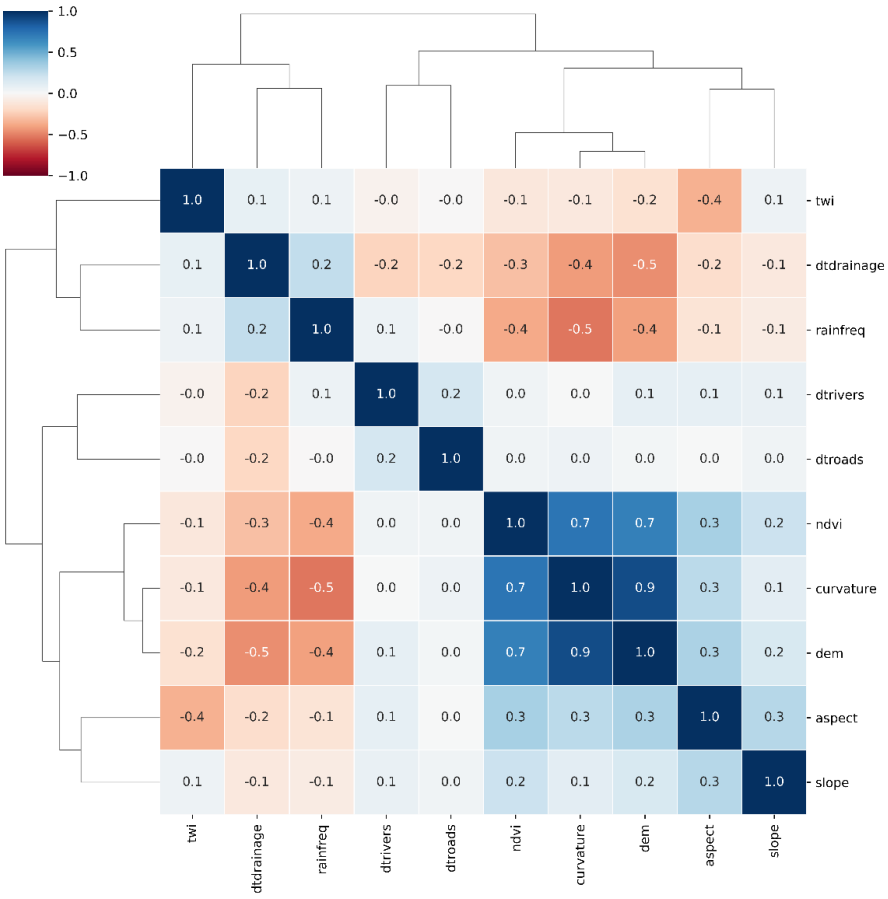

Figure 4 Hierarchical cluster-based Pearson correlation matrix of the ten flood conditioning features. All retained features satisfy independence criteria (inter-feature $r < 0.75$; VIF < 10).

2.4. Machine Learning model development

The preprocessed FCF stack was used to train and compare three gradient boosting algorithms based on literature review for flood susceptibility mapping. A stratified sample of 20,000 points was extracted from the WRI Aqueduct flood inventory, including 10,000 flood points and 10,000 non-flood points. The dataset was divided into 15,400 training points and 4,600 hold-out validation points, while Bayesian hyperparameter tuning was conducted within a 10-fold stratified cross-validation framework using ROC-AUC as the optimization target.

2.5. Model Internal Validation

Accurate validation of flood susceptibility models is essential to ensure predictive reliability and practical applicability [33]. Therefore, our model performance was evaluated using five complementary metrics: Accuracy, Precision, Recall, F1-Score, and ROC-AUC, computed from the confusion matrix entries using Equations (5-8).

$$\text{Accuracy} = \frac{TP + TN}{TP + TN + FP + FN} \tag{5}$$

$$\text{Precision} = \frac{TP}{TP + FP} \tag{6}$$

$$\text{Recall} = \frac{TP}{TP + FN} \tag{7}$$

$$\text{F1} = \frac{2 \times \text{Precision} \times \text{Recall}}{\text{Precision} + \text{Recall}} \tag{8}$$

where TP, TN, FP, and FN denote true positives, true negatives, false positives, and false negatives, respectively. ROC-AUC quantifies the model's ability to distinguish between flooded and non-flooded areas across all classification thresholds, with values approaching 1.0 indicating excellent discrimination and values near 0.5 reflecting performance no better than random chance. ROC-AUC was estimated using stratified 10-fold cross-validation to ensure robust generalization across spatial subsets. In addition to these five primary metrics, Balanced Accuracy and a composite Adjusted Score, computed as the mean of all normalized per-metric values across the seven indicators, were calculated as supplementary diagnostics to account for class imbalance and support objective cross-model comparison and final model selection

2.6. SHAP-based model interpretability

While gradient boosting models deliver strong predictive performance, their internal decision logic is not directly interpretable, limiting the physical understanding of which landscape factors drive flood susceptibility and how. To address this black-box limitation, SHapley Additive exPlanations (SHAP) analysis [34] was applied to the selected LightGBM model to quantify the marginal contribution of each FCF to individual flood susceptibility predictions. For a given model output$f(\boldsymbol{x})$, SHAP expresses the prediction using Equation (9).

$$f(x) \; = \; \varphi_0 \; + \; \sum_{j=1}^{M} \varphi_j \tag{9}$$

where ϕ_0 is the base rate (mean model output across all training samples), ϕ_j is the SHAP value for feature j representing its marginal contribution, and $M = 10$ is the total number of features. Global feature importance was summarized as mean absolute SHAP values ($\overline{|\phi_j|}$) across 20,000 training samples. SHAP dependence plots and beeswarm plots characterized non-linear feature-prediction relationships across Iowa's spatial domain. The trained LightGBM model was applied to the full 30 m raster stack across Iowa, producing a continuous flood susceptibility surface classified into five equal-interval classes [35]: Very Low (0.0–0.2), Low (0.2–0.4), Moderate (0.4–0.6), High (0.6–0.8), and Very High (0.8–1.0). The resulting flood susceptibility map (FSM) represents a relative hazard index on [0,1].

2.7. Agricultural Flood Risk Framework

2.7.1. Agriculture Exposure

Agricultural exposure (E) was quantified from four indicator surfaces derived from the USDA Census of Agriculture 2022: corn harvested acreage, soybean harvested acreage, corn gross economic value, and soybean gross economic value. Production volume layers were excluded from the exposure composite to avoid double-counting with economic value surfaces. All four indicators were normalized to [0,1] using 2nd–98th percentile clipping [36]. County-level USDA indicators were joined to county polygons and rasterized to 30 m resolution so that all pixels within a county inherited the same normalized county score. Because the USDA Census of Agriculture reports county totals rather than field-scale locations, these exposure surfaces are intended for comparative county-level screening and do not represent within-county field-level variability.

2.7.2. Socioeconomic Vulnerability

Socioeconomic vulnerability (V) was operationalized as an equal-weight composite of five USDA Census of Agriculture 2022 indicators: (i) tenant farming percentage; (ii) average farm size (inverted, so that smaller farms score higher); (iii) cropland intensity ratio; (iv) net cash farm income per operation (inverted); and (v) commodity sales per operation as an asset exposure proxy. Each indicator was normalized to [0,1] using the same percentile-clipping approach as the exposure layer. The composite vulnerability index was computed using Equation (10).

$$V = \frac{1}{5}\sum_{i=1}^{5} V_i \tag{10}$$

where V_i is the normalized score for vulnerability indicator i. Equal weighting was adopted as a transparent baseline consistent with prior composite vulnerability indices in the agricultural disaster risk literature [16].

2.7.3. Risk modeling framework

Agricultural flood risk was quantified using a multiplicative hazard–exposure–vulnerability framework as mentioned in Equation (11).

$$Risk = H \times E \times V \tag{11}$$

where H is the pixel-level LightGBM flood susceptibility value (0–1), E is the normalized agricultural exposure score, and V is the normalized composite socioeconomic vulnerability index. Four primary risk surfaces were produced: corn area risk, soybean area risk, corn economic risk, and soybean economic risk. A fifth combined economic risk surface was computed as the mean of the two economic surfaces. Raw multiplicative products were preserved without post-multiplication re-normalization. Risk surfaces were classified using quantile thresholds at the 20th, 40th, 60th, and 80th county-level percentiles.

In addition to the relative risk surfaces, a scenario-based expected annual agricultural loss index was estimated at the county level provided in Equation (12).

$$L_i = V\,AR_i \times P_{flood,i} \times (1 - C_{ins}) \tag{12}$$

where $L_i$is the expected annual loss for county i(USD/year), $VAR_i$is gross crop revenue (USD/year), $P_{flood,i}$is a scenario-based flood-probability proxy obtained by linearly rescaling mean county susceptibility to the range 0.05–0.35, and $C_{ins}$is the insurance coverage fraction (0.78 for Iowa based on USDA RMA 2022 averages). Because $P_{flood,i}$is derived from the susceptibility surface rather than from actuarial flood-frequency data, the resulting loss estimates should be interpreted as comparative planning indicators, not as calibrated empirical expected annual losses.

2.7.4. Spatial Hotspot Analysis

Lastly, Getis-Ord G_i^* spatial autocorrelation analysis was applied to identify statistically significant clusters of elevated agricultural flood risk [37]. The G_i^* statistic for county i is defined by Equation (13).

$$G_i^* = \frac{\sum_{j=1}^{n} w_{ij}\, x_j \; - \; \bar{x} \sum_{j=1}^{n} w_{ij}}{S \sqrt{\frac{n \sum_{j=1}^{n} w_{ij}^2 - (\sum_{j=1}^{n} w_{ij})^2}{n-1}}} \tag{13}$$

where x_j is the risk value for county j, w_{ij} is the row-standardized queen contiguity spatial weight, $\bar{x}$ is the mean risk value across all $n = 99$ counties, and S is the standard deviation of county risk values. Statistical significance was assessed at 90%, 95%, and 99% confidence levels using permutation inference with 999 permutations.

3. Results

3.1. Flood hazard pattern used for agricultural risk screening

LightGBM demonstrated the strongest overall predictive performance among the tested gradient boosting models and was therefore selected as the susceptibility layer for the subsequent agricultural flood risk analysis (Figure S1-S2, Table S1). The model achieved Accuracy = 0.88, Precision = 0.88, Recall = 0.87, F1-score = 0.90, and ROC-AUC = 0.95, indicating strong discriminatory ability and stable generalization across validation folds (more details are provided in Supplementary Table S1). SHAP interpretation further showed that the selected model remained physically meaningful, with elevation emerging as the dominant predictor, followed by rainfall frequency and hydrological proximity variables, particularly distance to rivers and drainage networks (Figure 5c). These results support the use of LightGBM not only as the best-performing model, but also as an interpretable basis for downstream hazard-exposure-vulnerability integration.

The final LightGBM flood susceptibility map indicates that most of Iowa falls within the very low susceptibility class (72.1%), while 8.7% is classified as low, 5.9% as moderate, 5.3% as high, and 8.0% as very high (Figure 5a,b). Taken together, the high and very high classes account for 13.3% of the state, forming the principal hazard belt used for agricultural risk screening. Spatially, these higher-susceptibility zones are concentrated along the Cedar River watershed, the Missouri River corridor, and the Mississippi River floodplain, highlighting the parts of Iowa where flood-prone landscapes most strongly intersect productive agricultural systems. In this study, the susceptibility surface is therefore treated not as an endpoint in itself,

but as the hazard foundation, for identifying where agricultural losses are more likely to concentrate.

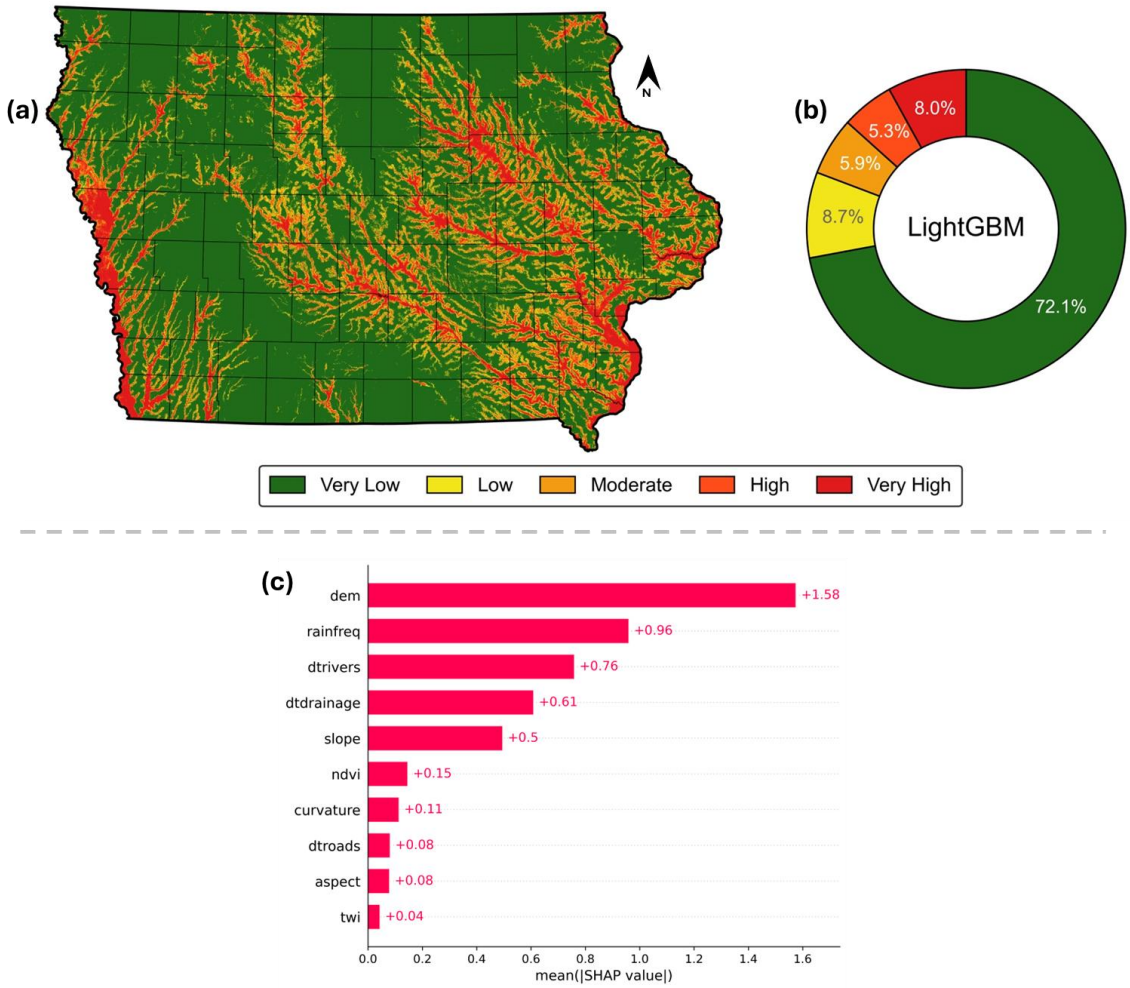

Figure 5 (a) Flood susceptibility spatial map for Iowa state, using best model (LightGBM), (b) susceptibility distribution percentage per class, and (c) SHAP model interpretation (mean |SHAP| values).

3.2. Agricultural exposure and vulnerability baseline

Iowa's agricultural baseline reveals both a large concentration of crop value and substantial inter-county differences in structural vulnerability. Based on the 2022 USDA Census of Agriculture, the state's corn-soybean system represents a combined gross agricultural exposure of $17.60 billion annually, comprising $11.37 billion from corn and $6.23 billion from soybeans. Corn also dominates in harvested area, with 12,791,132 acres compared with 9,580,405 acres for soybeans (Table S2). At the county level, Kossuth records the highest corn acreage (304,643 acres), while Pottawattamie records the highest soybean acreage (221,329 acres), confirming that exposure is unevenly distributed across Iowa rather than uniformly shared among counties (Figure 6a). This uneven crop-value geography provides the essential exposure baseline for interpreting later differences in county-scale flood risk.

Composite agricultural vulnerability shows a different, but equally important, spatial structure (Figure 6b). The composite vulnerability index has a statewide mean of 0.549 ± 0.093, indicating moderate but spatially variable vulnerability across Iowa's 99 counties. Among the

five indicators, cropland intensity is the dominant contributor (normalized mean = 0.717), followed by farm income vulnerability (0.610), average farm size vulnerability (0.552), tenant farming rate (0.536), and the asset sales proxy (0.328) (Figure 6c). The highest composite vulnerability is observed in Osceola County (0.756), with other highly vulnerable counties including Polk, O'Brien, Franklin, and Black Hawk. Importantly, the spatial distribution of vulnerability does not mirror the flood susceptibility pattern directly, which reinforces the need for an integrated HEV framework rather than hazard-only screening. In other words, counties with the highest agricultural flood concern are not defined by hazard alone, but by the intersection of flood-prone landscapes with concentrated crop value and structurally vulnerable farm systems. More details on individual crop exposure assessments are provided in Supplementary file as Figure S3-S4.

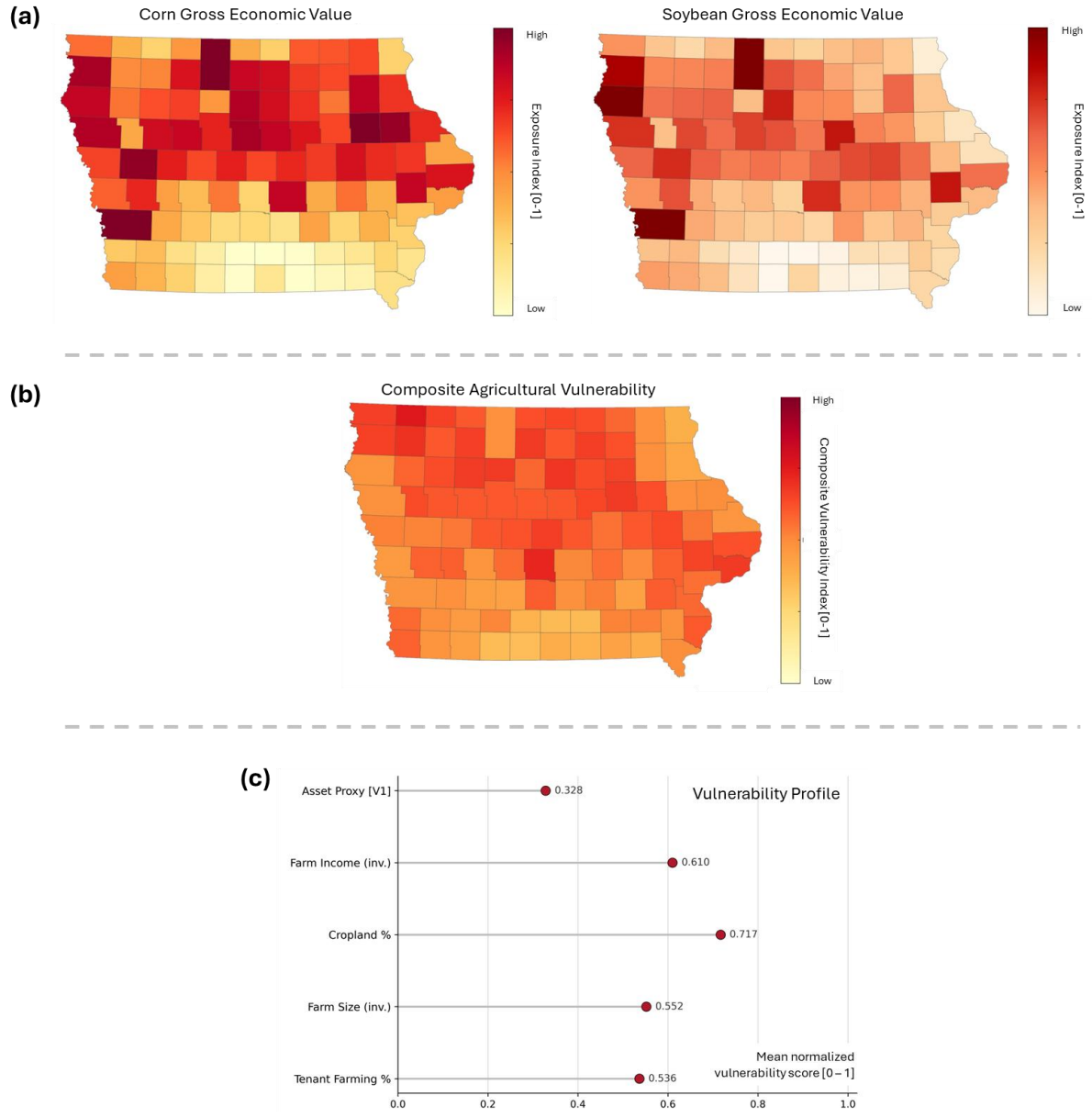

Figure 6 Agricultural exposure–vulnerability baseline across Iowa: (a) county-level corn gross economic value and soybean gross economic value (normalized); (b) composite agricultural vulnerability index; and (c) mean normalized scores of the five vulnerability indicators across the 99 counties.

3.3. Integrated agricultural flood risk across counties

Integrated HEV analysis revealed a clear concentration of agricultural flood risk in east-central Iowa, particularly within the Cedar River watershed, with additional high-risk counties extending along the western Missouri River corridor (Figure 7). At the statewide level, the mean combined economic risk index was 0.054, with a maximum of 0.587, while corn economic risk (mean = 0.058; max = 0.619) remained consistently higher than soybean economic risk (mean = 0.049; max = 0.580). This pattern indicates that the state's agricultural flood burden is not evenly distributed but instead concentrates where elevated hazard intersects high-value crop systems and structurally vulnerable farm conditions.

At the county level, Black Hawk County recorded the highest combined economic risk index (0.191), followed by Monona (0.160), Clinton (0.149), Linn (0.143), and Marshall (0.135) (Figure 7b). Black Hawk's leading position reflects the convergence of moderate-to-high flood susceptibility with substantial crop exposure and an elevated composite vulnerability score, making it the clearest example of compound agricultural flood risk in the state. By contrast, Monona represents a different risk structure, where very high hazard along the Missouri River corridor intersects extensive crop exposure, particularly corn acreage, to produce a similarly high county-scale risk score. These results show that high county-level agricultural flood risk emerges where flood susceptibility, crop value, and socioeconomic vulnerability overlap, although the relative contribution of each component differs among counties. The highest-risk counties are concentrated in east-central Iowa and along parts of the Missouri River corridor.

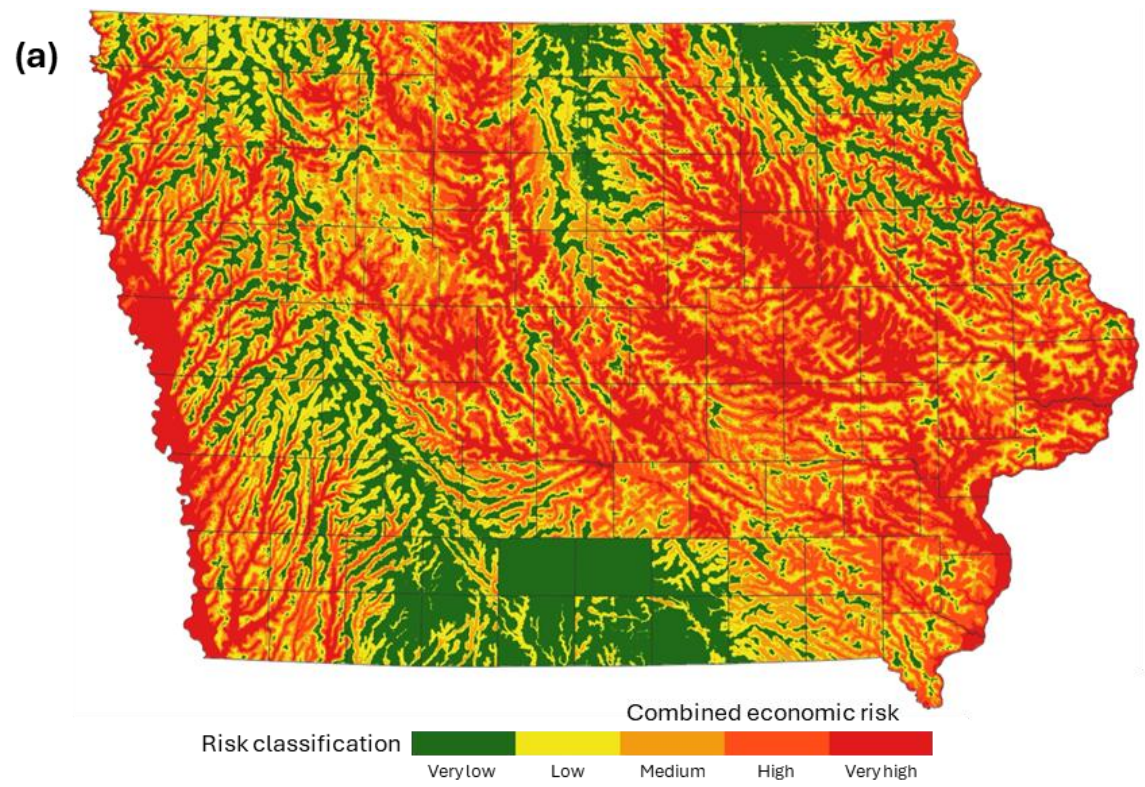

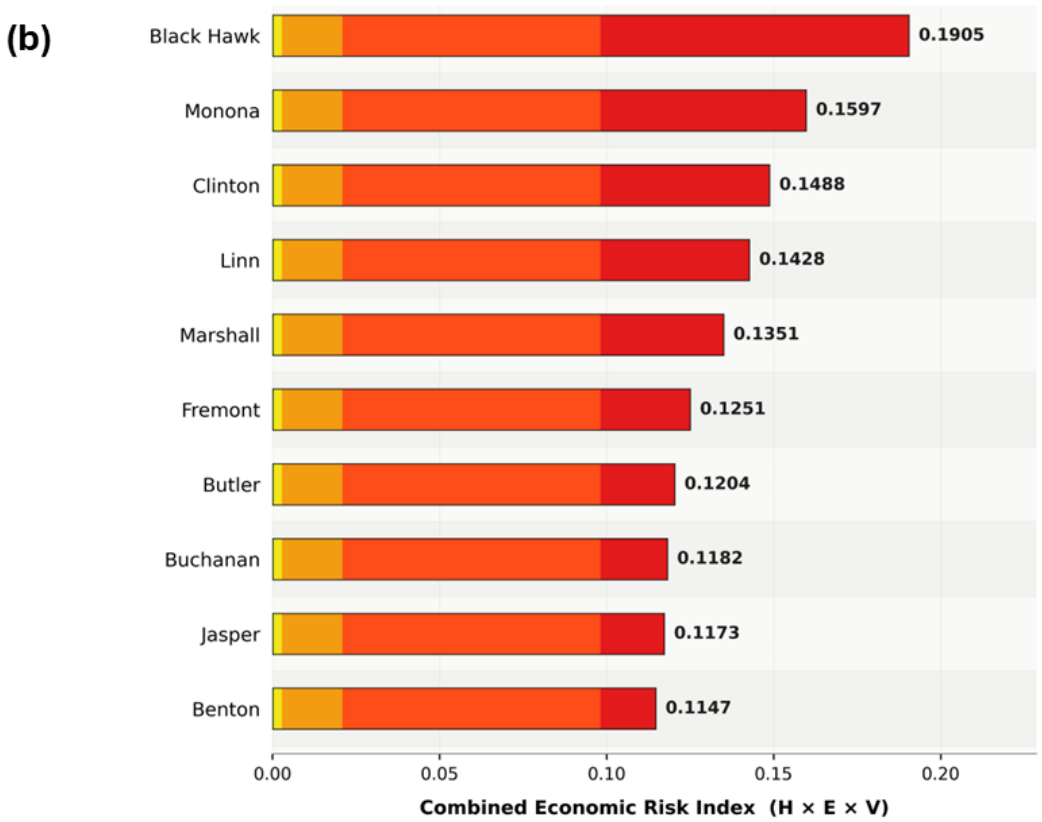

Figure 7 Integrated agricultural flood risk across Iowa under the HEV framework: (a) combined economic risk map derived from the mean of corn and soybean economic risk surfaces; (b) top counties ranked by combined economic risk index. High-risk counties are concentrated in east-central Iowa, particularly within the Cedar River watershed, with additional high-risk areas along the Missouri River corridor.

3.4. Scenario-based loss and county prioritization

Scenario-based annualized agricultural flood loss was estimated at $527.7 million per year across Iowa, equivalent to 3.04% of gross crop revenue, indicating a substantial statewide flood burden on the corn–soybean production system (Figure 8a-b). Of this total, corn accounts for $353.8 million per year and soybean for $173.9 million per year, showing that corn contributes the larger share of expected loss under the present scenario-based framework (Table S3). At the county level, loss estimates are strongly concentrated rather than uniformly distributed, with the most affected counties aligned primarily along the Missouri River corridor and other major flood-prone agricultural zones.

Monona County recorded the highest scenario-based annualized loss at $19.9 million per year, followed by Pottawattamie ($13.2 million) and Harrison ($12.4 million) (Figure 8a-b). Monona's position reflects the intersection of very high flood susceptibility with extensive corn acreage, while the other leading loss counties also combine high agricultural exposure with elevated flood likelihood. These results complement, but do not duplicate, the integrated risk findings: counties with the highest composite risk are not always those with the largest absolute expected loss, because loss magnitude is additionally shaped by the scale of crop value at risk. This distinction is important for policy because it separates structurally compound risk from purely exposure-driven loss concentration.

County prioritization further revealed a strongly polarized agricultural flood landscape across Iowa (Figure 8c). Using median thresholds of combined economic risk and expected annualized loss, 48 counties were classified as Priority 1 (high risk, high loss) and 47 counties as Priority 4 (low risk, low loss), while only 2 counties each fell into Priorities 2 and 3 (Table S4). The five highest-risk Priority 1 counties were Black Hawk, Monona, Clinton, Linn, and Marshall, confirming that the state's most urgent intervention areas are concentrated where flood susceptibility, agricultural value, and vulnerability converge. Together, the loss and typology results distinguish counties requiring immediate adaptation and insurance attention from counties where baseline monitoring and lower-intensity preparedness may be sufficient.

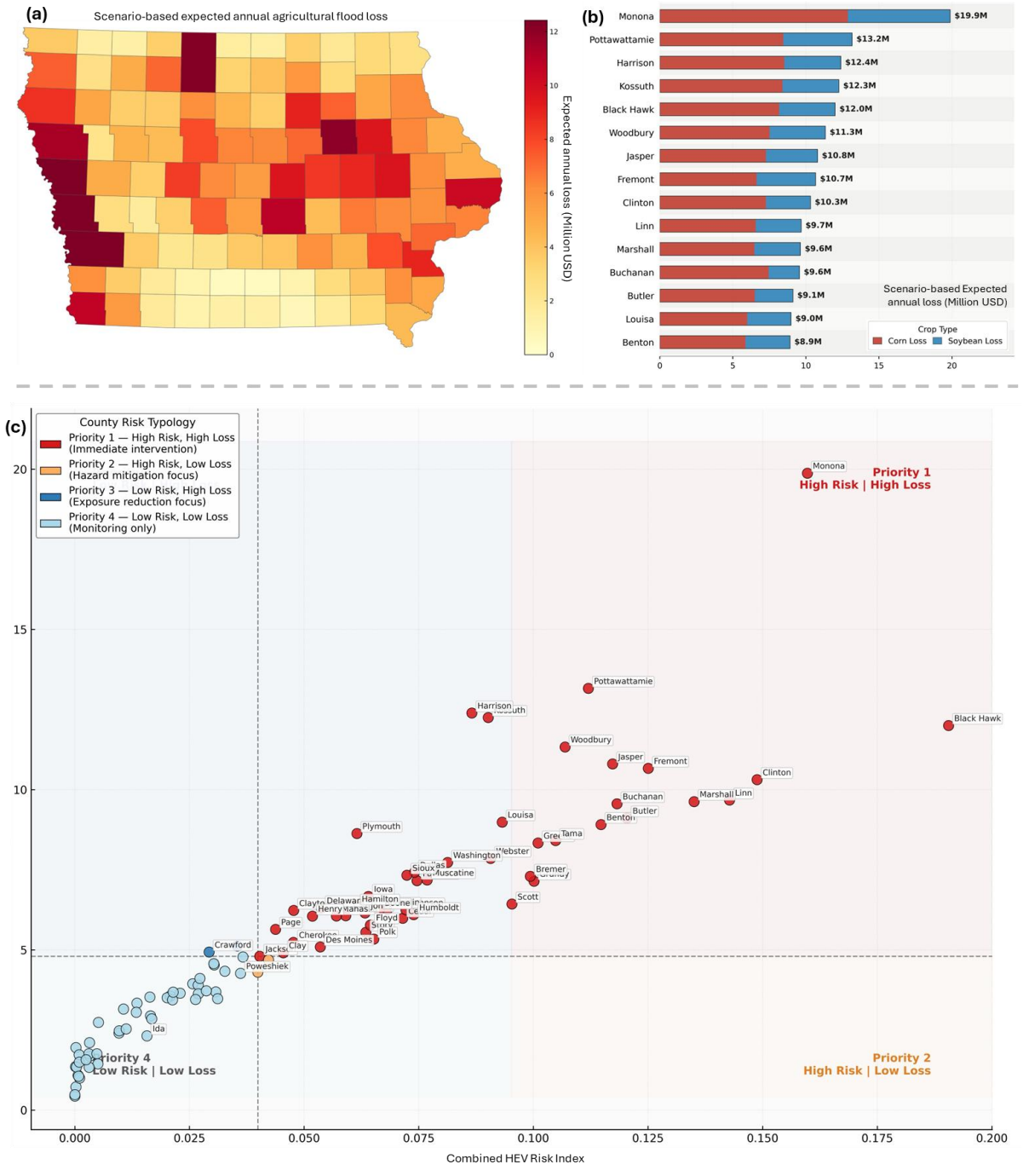

Figure 8 Scenario-based annualized agricultural flood loss and county prioritization across Iowa: (a) county-level annualized loss choropleth; (b) corn and soybean loss breakdown for the top 15 counties by total annualized loss; (c) county typology based on state median thresholds of combined economic risk and annualized loss, showing Priority 1–4 intervention classes.

3.5. Persistent hotspots and consistency checks

Getis-Ord Gi* analysis revealed a pronounced and persistent spatial clustering of agricultural flood risk in east-central Iowa, centered on the Cedar River watershed (Figure 9a). For corn economic risk, seven counties reached 99% hotspot confidence, namely Cedar, Black Hawk, Benton, Grundy, Buchanan, Tama, and Bremer. For soybean economic risk, seven counties also reached 99% hotspot confidence: Cedar, Black Hawk, Poweshiek, Benton, Johnson, Grundy, and Tama. Across all three dimensions examined, a common cluster of 13 counties emerged as persistent hotspots, indicating that elevated agricultural flood risk in Iowa is not randomly distributed, but strongly concentrated within a coherent regional corridor. This east-central hotspot concentration is one of the most spatially important findings of the study because it identifies where high hazard, high agricultural value, and elevated vulnerability repeatedly converge.

In contrast, southern Iowa showed persistent low-risk clustering, with several counties appearing as statistically significant coldspots, particularly for corn economic risk (Figure 9b). This strong hotspot–coldspot contrast reinforces the spatial polarization already observed in the county typology results and further supports the interpretation that agricultural flood risk in Iowa is driven by geographic co-location of multiple risk dimensions rather than by any single component in isolation. From a disaster-risk-reduction perspective, the Cedar River watershed hotspot belt therefore represents the clearest regional target for concentrated mitigation, adaptation planning, and agricultural risk-management intervention.

Consistency checks further indicated that the integrated framework is spatially coherent. The combined economic risk index was strongly correlated with LightGBM flood susceptibility across counties (Spearman $r_s = 0.793$, $p < 0.0001$), while scenario-based annualized loss was very strongly correlated with the combined risk index ($r_s = 0.976$, $p < 0.0001$). Total annualized loss also showed a moderate positive relationship with total harvested crop area ($r_s = 0.630$, $p < 0.0001$), and the more modest correlation between vulnerability and the risk index ($r_s = 0.345$, $p = 0.0005$) indicates that vulnerability contributes meaningfully without simply duplicating the hazard pattern. Together, these relationships support the internal consistency of the HEV framework and confirm that the final risk outputs behave in a spatially rational way. To complement the hotspot analysis, Table 2 summarizes county-level consistency and benchmark checks for the integrated HEV framework.

Comparison with USDA RMA 2022 all-peril corn–soybean indemnity payments produced a non-significant association ($r_s = -0.070$, $p = 0.494$), but this mismatch is methodologically expected rather than contradictory (Figure S5). The RMA dataset reflects all insured perils rather than flood alone, 2022 was drought-dominated in northwest Iowa, and the present framework estimates long-run scenario-based annualized flood loss rather than losses from a single year. Accordingly, the benchmark comparison should be interpreted as a limited external reference rather than a direct flood-loss validation.

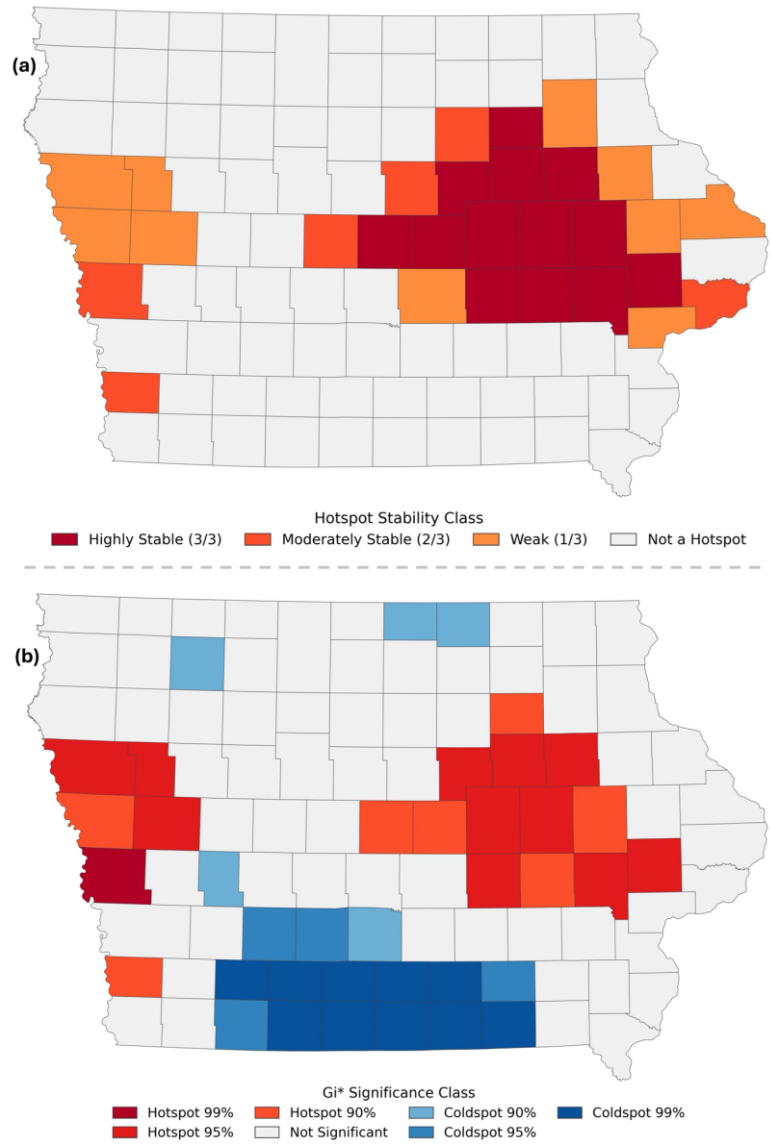

Figure 9 Spatial concentration of agricultural flood risk across Iowa based on Getis–Ord Gi* analysis: (a) hotspot stability classes showing counties identified as hotspots across one, two, or all three analyzed risk dimensions; and (b) hotspot/coldspot significance classes illustrating the spatial polarization of county-level agricultural flood risk, with a dominant hotspot belt in east-central Iowa and persistent coldspots in the south.

Table 2 County-level consistency and benchmark checks for the HEV agricultural flood risk framework in Iowa.

Comparison	**Spearman r_s**	**p-value**	**Interpretation**
LightGBM flood susceptibility vs. combined economic risk index	0.793	<0.0001	Strong positive association
Combined economic risk index vs. scenario-based annualized loss	0.976	<0.0001	Very strong positive association
Total harvested crop area vs. total annualized loss	0.630	<0.0001	Moderate positive association
Composite vulnerability index vs. combined economic risk index	0.345	0.0005	Modest positive association
USDA RMA 2022 all-peril corn–soybean indemnity payments vs. scenario-based annualized flood loss	-0.070	0.494	Non-significant association

4. Discussion

This study advances county-scale integrated agricultural flood risk assessment in Iowa by combining a continuous ML-derived susceptibility, crop-specific economic exposure, and socioeconomic vulnerability within a unified HEV framework. The discussion below interprets these findings in relation to prior Iowa flood studies and the broader GeoAI flood-risk literature, with emphasis on what the framework reveals about spatial risk differentiation, scenario-based crop loss, and county-level prioritization.

4.1. Model performance and hazard layer

LightGBM's superiority over XGBoost and HistGBM (ROC-AUC = 0.95 vs. 0.94 and 0.93) is consistent with comparable gradient boosting benchmarks in the flood susceptibility literature. Recent studies reported analogous LightGBM advantages in a 14-model comparison, attributing them to GOSS and EFB's capacity to handle class imbalance in sparse flood inventories [3,20]. The ROC-AUC of 0.95 falls within the 0.91–0.97 range reported by across global flood susceptibility studies, confirming that performance is robust and consistent with recent studies for gradient boosting applied to binary flood classification [38]. Cross-model spatial consistency, with all three models classifying 13.0–13.3% of Iowa as High or Very High susceptibility, reinforces confidence that this estimate reflects genuine landscape properties rather than model-specific artifacts.

The SHAP attribution hierarchy, with elevation, rainfall frequency, and river proximity as dominant predictors, aligns with the physical hydrology of Iowa's glacially derived, low-relief terrain. Elevation's dominance (mean |SHAP| = 1.58) reflects the concentration of high-susceptibility zones in river floodplains and glacially formed swales, where topographic variation of even a few meters substantially alters inundation probability. Rainfall frequency's high rank is consistent with Iowa's position at the intersection of Gulf moisture advection and continental precipitation variability. This physically interpretable attribution helps address the black-box limitation often associated with machine-learning-based flood susceptibility studies [16,39] and supports the physical plausibility of the final susceptibility surface.

4.2. HEV integration and risk differentiation

The use of a continuous LightGBM susceptibility surface, rather than static FEMA 100-year floodplain extents, enables risk estimation across the full spatial gradient of flood probability. This moves the analysis beyond a binary floodplain designation toward a spatially differentiated hazard representation. Yildirim et al. (2022) used FEMA extents as their hazard layer and acknowledged that this approach systematically underrepresents risk in low-lying areas outside designated floodways. Alabbad & Demir (2024) applied fuzzy overlay analysis to built-environment exposure across multiple return period scenarios but explicitly identified the absence of vulnerability assessment and agricultural economic loss integration as key gaps. The present framework addresses both limitations in a unified approach, producing a spatially richer and more policy-actionable risk profile.

From a disaster risk reduction perspective, the framework has three immediate applications. First, it can support county-level prioritization of mitigation resources by distinguishing structurally compound risk from purely exposure-driven loss concentration. Second, the hotspot and typology outputs can inform watershed-scale adaptation planning, including

floodplain restoration, drainage and retention interventions, crop insurance targeting, and extension-based resilience support in repeatedly affected counties. Third, because the framework integrates hazard, agricultural value, and farm-system vulnerability, it provides a more decision-relevant basis for screening where flood impacts are most likely to threaten agricultural continuity and local rural livelihoods than hazard-only mapping alone.

Black Hawk County's emergence as the highest combined economic risk county (index = 0.191) despite not recording the highest loss illustrates the analytical value of separating composite risk from loss magnitude. Black Hawk's elevated index reflects the convergence of Cedar River flood susceptibility with high cropland intensity and elevated tenant farming rates, representing a structurally compound risk that no single-dimension analysis can detect. Monona County's lead in expected annual loss ($19.9M/year), by contrast, reflects extreme susceptibility along the Missouri River corridor intersecting large corn acreage, an exposure-driven profile rather than a vulnerability-driven one. These contrasting county profiles suggest that high agricultural flood risk in Iowa is not generated through a single pathway. In some counties, risk is amplified more strongly by structural vulnerability, whereas in others it is driven more directly by the co-location of very high hazard and concentrated crop exposure. This distinction is important because it indicates that county-level adaptation priorities may differ even when overall risk values are similarly high.

4.3. Economic loss estimation and policy relevance

The total scenario-based expected annual agricultural flood loss of $527.7 million, equivalent to 3.04% of gross crop revenue, places Iowa’s agricultural flood burden in a clear planning context. The crop-specific decomposition further shows that corn accounts for the larger share of scenario-based loss, indicating that the state’s dominant production system is also the most economically exposed under the present framework. Compared with earlier Iowa studies that emphasized aggregate exposure, this crop-level differentiation provides a more decision-relevant basis for understanding where agricultural flood losses may concentrate and which commodities contribute most to statewide risk.

4.4. The 13-county east-central hotspot cluster

The identification of a persistent 13-county hotspot cluster in east-central Iowa is one of the clearest spatial findings of this study. Centered on the Cedar River watershed, this cluster indicates that elevated agricultural flood risk is regionally concentrated rather than diffusely distributed across the state. In comparison with earlier Iowa studies that emphasized floodplain exposure or built-environment impacts, the present results show that the Cedar River corridor also emerges as a concentrated zone when hazard, crop value, and socioeconomic vulnerability are evaluated together.

The strongly bimodal county typology, with 48 Priority 1 and 47 Priority 4 counties and very few intermediate cases, further suggests that agricultural flood risk in Iowa is spatially polarized. Rather than varying smoothly from county to county, risk appears to intensify where multiple dimensions of hazard, exposure, and vulnerability co-locate. This makes the east-central hotspot belt a particularly important area for targeted monitoring, mitigation planning, and agricultural adaptation efforts.

4.5. Transferability and scalability

Another major strength of the framework is its transferability. Because it is built primarily from publicly available geospatial, census, and agricultural datasets, it can be updated for future census cycles and adapted to other Corn Belt states without requiring proprietary data inputs. More broadly, the workflow offers a scalable template for agricultural flood-risk screening in other intensively farmed flood-prone regions where hazard, exposure, and vulnerability data can be assembled at comparable spatial scales.

4.6. Limitations and Future Directions

Despite the strengths of the proposed framework, some methodological limitations should be considered when interpreting the results. First, the loss component remains scenario-based rather than actuarially calibrated. In the present study, county-level flood probability was approximated by linearly scaling mean LightGBM susceptibility values, which creates partial dependence between the hazard layer and the loss function. As a result, the estimated annualized agricultural losses should be interpreted as comparative planning indicators rather than direct empirical estimates of expected annual loss. Future work could strengthen this component by replacing the susceptibility-based proxy with independently derived flood-frequency information, such as return-period surfaces, gauge-based exceedance probabilities, or hydraulic inundation products. Second, the exposure and vulnerability components are constrained by the spatial resolution of the available agricultural statistics. The USDA Census of Agriculture provides robust county-level information, but it does not resolve sub-county variability in crop distribution, farm structure, or localized management practices. Consequently, exposure is spatially generalized within counties, which may mask finer-scale patterns of agricultural flood sensitivity. Integrating higher-resolution crop allocation products, such as parcel-level agricultural inventories or remotely sensed cropland datasets, would improve the spatial realism of future risk estimates.

Third, the vulnerability index was constructed using equal weighting across five indicators for transparency and reproducibility. While this approach provides a clear baseline, it does not fully capture the possibility that some structural factors may contribute more strongly than others to agricultural flood sensitivity in Iowa. Future studies could compare equal weighting with alternative schemes based on expert judgment, principal component analysis, analytic hierarchy process, or empirical calibration against observed post-flood agricultural impacts. Fourth, the external benchmarking used in this study remains limited. The weak relationship between the scenario-based flood loss estimates and 2022 USDA RMA indemnity payments is not unexpected, because the RMA records reflect all insured perils rather than flood alone, and 2022 was influenced strongly by drought conditions in parts of Iowa. A more rigorous external validation would require flood-specific indemnity records, historical county-level crop damage observations, or post-event agricultural loss surveys from flood-dominated years such as 2008 or 2019.

Finally, the framework should be viewed as dynamic rather than fixed. Because agricultural exposure, commodity prices, insurance participation, and farm structural conditions change over time, the resulting risk patterns will also evolve. Future work should therefore update the

framework using newer Census of Agriculture releases, annual NASS production statistics, and event-specific flood observations. Extension of the same workflow to neighboring Corn Belt states would also provide an important test of regional transferability and would help determine whether the hazard-exposure-vulnerability relationships identified in Iowa are consistent across other intensive agricultural landscapes.

5. Conclusion

This study presents an integrated GeoAI-based framework for county-scale agricultural flood risk assessment in Iowa by combining machine-learning-derived flood susceptibility, crop-specific economic exposure, and socioeconomic vulnerability within a hazard-exposure-vulnerability (HEV) framework. In contrast to susceptibility-only or static floodplain-based approaches, the framework captures how flood risk intensifies where susceptible landscapes, concentrated crop value, and structurally vulnerable farm systems intersect.

LightGBM produced the most reliable susceptibility surface, with strong predictive performance and physically interpretable controls dominated by elevation, rainfall frequency, and hydrological proximity. The final susceptibility map showed that 13.3% of Iowa falls within high or very high flood susceptibility, concentrated mainly along the Cedar River watershed, the Missouri River corridor, and the Mississippi River floodplain. When integrated with county-level agricultural and socioeconomic data, these hazard patterns translated into a more differentiated and policy-relevant risk geography. Black Hawk County emerged as the highest combined agricultural flood risk county, whereas Monona County recorded the highest scenario-based annualized loss, demonstrating that compound risk and absolute loss magnitude do not necessarily coincide.

The results further reveal a strong spatial concentration of agricultural flood risk across Iowa. A persistent east-central hotspot cluster centered on the Cedar River watershed, together with the identification of 48 Priority 1 counties, shows that flood risk is highly uneven and regionally clustered rather than uniformly distributed across the state. This is a key contribution because it provides a clearer basis for targeting adaptation, mitigation, and agricultural risk-management efforts than conventional hazard screening alone.

Overall, the study demonstrates that integrating interpretable machine learning with agricultural exposure and vulnerability metrics can produce a more actionable understanding of flood risk in intensive farming systems. Although the loss estimates are scenario-based and should be interpreted as comparative planning indicators rather than actuarial values, the framework is scalable, transferable, and readily updateable using public datasets. It therefore offers a practical foundation for supporting disaster risk reduction, climate adaptation, and flood-risk-informed agricultural planning in Iowa and other flood-prone agricultural regions.

CRediT Authorship Contribution Statement

Mirza Md Tasnim Mukarram: Conceptualization, Data curation, Formal analysis, Investigation, Methodology, Visualization, Writing – original draft. Mirza Waleed: Conceptualization, Methodology, Software, Formal analysis, Visualization, Writing – review & editing, Supervision, Project administration, Funding acquisition. Quazi Umme Ruki:

Investigation, Data curation, Writing – original draft. Marc Linderman: Supervision, Writing – review & editing. Ibrahim Demir: Supervision, Writing – review & editing.

Acknowledgements

The authors gratefully acknowledge the providers of the openly accessible datasets and platforms used in this study, including the USDA National Agricultural Statistics Service (NASS), Google Earth Engine, FABDEM, CHIRPS, HydroSHEDS, OpenStreetMap, and the WRI Aqueduct Flood Analyzer. Their publicly available data resources made this county-scale agricultural flood risk assessment possible.

The corresponding author, Mirza Waleed, gratefully acknowledges Hong Kong Baptist University for support toward the article processing charge (APC) of this paper. He also acknowledges support through a PhD Studentship (2022–2026).

Data and Code Availability

Code supporting this study is openly available at the GitHub repository Agricultural-Flood-Risk: https://github.com/Mirza9003/Agricultural-Flood-Risk. The analysis is based primarily on publicly available datasets, including USDA NASS Census of Agriculture and QuickStats, FABDEM, CHIRPS, HydroSHEDS, OpenStreetMap, Landsat-derived products, and the WRI Aqueduct Flood Analyzer. Derived outputs and supplementary materials are available from the corresponding author upon reasonable request.

Declaration of Competing Interest

The authors declare that they have no known competing financial interests or personal relationships that could have appeared to influence the work reported in this paper.

References

[1] J.S. Rogers, M.P. Maneta, S.R. Sain, L.E. Madaus, J.P. Hacker, The role of climate and population change in global flood exposure and vulnerability, Nat Commun 16 (2025) 1287. https://doi.org/10.1038/s41467-025-56654-8.

[2] B.A. Cikmaz, E. Yildirim, I. Demir, Flood susceptibility mapping using fuzzy analytical hierarchy process for Cedar Rapids, Iowa, International Journal of River Basin Management 23 (2025) 1–13. https://doi.org/10.1080/15715124.2023.2216936.

[3] M. Waleed, M. Sajjad, Advancing flood susceptibility prediction: A comparative assessment and scalability analysis of machine learning algorithms via artificial intelligence in high-risk regions of Pakistan, Journal of Flood Risk Management 18 (2025) e13047. https://doi.org/10.1111/jfr3.13047.

[4] A.R. Scorzini, M. Di Bacco, G. Manella, Regional flood risk analysis for agricultural crops: Insights from the implementation of AGRIDE-c in central Italy, International Journal of Disaster Risk Reduction 53 (2021) 101999. https://doi.org/10.1016/j.ijdrr.2020.101999.

[5] C.A. Grant, Y. Alabbad, E. Yildirim, I. Demir, Comprehensive Assessment of Flood Risk and Vulnerability for Essential Facilities: Iowa Case Study, Urban Science 8 (2024). https://doi.org/10.3390/urbansci8030145.

[6] E. Yildirim, C. Just, I. Demir, Flood risk assessment and quantification at the community and property level in the State of Iowa, International Journal of Disaster Risk Reduction 77 (2022) 103106. https://doi.org/10.1016/j.ijdrr.2022.103106.
[7] E. Yildirim, I. Demir, An Integrated Flood Risk Assessment and Mitigation Framework: A Case Study for Middle Cedar River Basin, Iowa, US, International Journal of Disaster Risk Reduction 56 (2021) 102113. https://doi.org/10.1016/j.ijdrr.2021.102113.
[8] E. Tate, M.A. Rahman, C.T. Emrich, C.C. Sampson, Flood exposure and social vulnerability in the United States, Nat Hazards 106 (2021) 435–457. https://doi.org/10.1007/s11069-020-04470-2.
[9] H. Darabi, B. Choubin, O. Rahmati, A. Torabi Haghighi, B. Pradhan, B. Kløve, Urban flood risk mapping using the GARP and QUEST models: A comparative study of machine learning techniques, Journal of Hydrology 569 (2019) 142–154. https://doi.org/10.1016/j.jhydrol.2018.12.002.
[10] B.T. Pham, C. Luu, D.V. Dao, T.V. Phong, H.D. Nguyen, H.V. Le, J. von Meding, I. Prakash, Flood risk assessment using deep learning integrated with multi-criteria decision analysis, Knowledge-Based Systems 219 (2021) 106899. https://doi.org/10.1016/j.knosys.2021.106899.
[11] A.J. Miller, M.E. Arias, S. Alvarez, Built environment and agricultural value at risk from Hurricane Irma flooding in Florida (USA), Nat Hazards 109 (2021) 1327–1348. https://doi.org/10.1007/s11069-021-04880-w.
[12] D. Ahmad, M. Afzal, Flood hazards and agricultural production risks management practices in flood-prone areas of Punjab, Pakistan, Environ Sci Pollut Res 29 (2022) 20768–20783. https://doi.org/10.1007/s11356-021-17182-2.
[13] M. Raza, A.A. Hatab, Assessment of vulnerability and resilience of smallholder farming households to flood risks: Insights from the Southern Punjab region of Pakistan, International Journal of Disaster Risk Reduction 126 (2025) 105600. https://doi.org/10.1016/j.ijdrr.2025.105600.
[14] E. Yildirim, I. Demir, Agricultural flood vulnerability assessment and risk quantification in Iowa, Science of The Total Environment 826 (2022) 154165. https://doi.org/10.1016/j.scitotenv.2022.154165.
[15] Y. Alabbad, I. Demir, Comprehensive flood vulnerability analysis in urban communities: Iowa case study, International Journal of Disaster Risk Reduction 74 (2022) 102955. https://doi.org/10.1016/j.ijdrr.2022.102955.
[16] Y. Alabbad, I. Demir, Geo-spatial analysis of built-environment exposure to flooding: Iowa case study, Discov Water 4 (2024) 28. https://doi.org/10.1007/s43832-024-00082-0.
[17] M. Eini, H.S. Kaboli, M. Rashidian, H. Hedayat, Hazard and vulnerability in urban flood risk mapping: Machine learning techniques and considering the role of urban districts, International Journal of Disaster Risk Reduction 50 (2020) 101687. https://doi.org/10.1016/j.ijdrr.2020.101687.
[18] R. Costache, Flood Susceptibility Assessment by Using Bivariate Statistics and Machine Learning Models - A Useful Tool for Flood Risk Management, Water Resour Manage 33 (2019) 3239–3256. https://doi.org/10.1007/s11269-019-02301-z.
[19] J. Chen, G. Huang, W. Chen, Towards better flood risk management: Assessing flood risk and investigating the potential mechanism based on machine learning models, Journal of Environmental Management 293 (2021) 112810. https://doi.org/10.1016/j.jenvman.2021.112810.
[20] M. Waleed, M. Sajjad, High-resolution flood susceptibility mapping and exposure assessment in Pakistan: An integrated artificial intelligence, machine learning and geospatial framework, International Journal of Disaster Risk Reduction 121 (2025) 105442. https://doi.org/10.1016/j.ijdrr.2025.105442.

[21] S. Bhere, M.J. Reddy, Flood risk assessment of suburban region in India by incorporating flood hazard, vulnerability and exposure, Nat Hazards 121 (2025) 6625–6649. https://doi.org/10.1007/s11069-024-07062-6.
[22] U.K. Mandal, F. Karim, Y. Yu, A. Ghosh, T. Zahan, S. Mallick, M. Kamruzzaman, P.L.C. Paul, M. Mainuddin, Assessing vulnerability and climate risk to agriculture for developing resilient farming strategies in the Ganges Delta, Climate Risk Management 47 (2025) 100690. https://doi.org/10.1016/j.crm.2025.100690.
[23] G. Antzoulatos, I.-O. Kouloglou, M. Bakratsas, A. Moumtzidou, I. Gialampoukidis, A. Karakostas, F. Lombardo, R. Fiorin, D. Norbiato, M. Ferri, A. Symeonidis, S. Vrochidis, I. Kompatsiaris, Flood Hazard and Risk Mapping by Applying an Explainable Machine Learning Framework Using Satellite Imagery and GIS Data, Sustainability 14 (2022). https://doi.org/10.3390/su14063251.
[24] Z. He, Z. Wu, O. Herzog, J. Hei, L. Li, X. Li, Compound health effects and risk assessment of extreme heat and ozone air pollution under climate change: A case study of 731 urban areas in China, Sustainable Cities and Society 119 (2025) 106084. https://doi.org/10.1016/j.scs.2024.106084.
[25] Y. Alabbad, J. Mount, A.M. Campbell, I. Demir, Assessment of transportation system disruption and accessibility to critical amenities during flooding: Iowa case study, Science of The Total Environment 793 (2021) 148476. https://doi.org/10.1016/j.scitotenv.2021.148476.
[26] Y. Alabbad, E. Yildirim, I. Demir, Flood mitigation data analytics and decision support framework: Iowa Middle Cedar Watershed case study, Science of The Total Environment 814 (2022) 152768. https://doi.org/10.1016/j.scitotenv.2021.152768.
[27] L. Hawker, P. Uhe, L. Paulo, J. Sosa, J. Savage, C. Sampson, J. Neal, A 30 m global map of elevation with forests and buildings removed, Environ. Res. Lett. 17 (2022) 024016. https://doi.org/10.1088/1748-9326/ac4d4f.
[28] B. Lehner, G. Grill, Global river hydrography and network routing: baseline data and new approaches to study the world's large river systems, Hydrological Processes 27 (2013) 2171–2186. https://doi.org/10.1002/hyp.9740.
[29] G. Boeing, Street Network Models and Indicators for Every Urban Area in the World, Geographical Analysis 54 (2022) 519–535. https://doi.org/10.1111/gean.12281.
[30] C. Funk, P. Peterson, M. Landsfeld, D. Pedreros, J. Verdin, S. Shukla, G. Husak, J. Rowland, L. Harrison, A. Hoell, J. Michaelsen, The climate hazards infrared precipitation with stations—a new environmental record for monitoring extremes, Sci Data 2 (2015) 150066. https://doi.org/10.1038/sdata.2015.66.
[31] S. Kuzma, M.F.P. Bierkens, S. Lakshman, T. Luo, L. Saccoccia, E.H. Sutanudjaja, R. Van Beek, Aqueduct 4.0: Updated Decision-Relevant Global Water Risk Indicators, WRIPUB (2023). https://doi.org/10.46830/writn.23.00061.
[32] NASS, USDA - National Agricultural Statistics Service - Census of Agriculture, (2022). https://www.nass.usda.gov/AgCensus/ (accessed April 4, 2026).
[33] Y. Bhattarai, S. Duwal, S. Sharma, R. Talchabhadel, Leveraging machine learning and open-source spatial datasets to enhance flood susceptibility mapping in transboundary river basin, International Journal of Digital Earth 17 (2024) 2313857. https://doi.org/10.1080/17538947.2024.2313857.
[34] S.M. Lundberg, G. Erion, H. Chen, A. DeGrave, J.M. Prutkin, B. Nair, R. Katz, J. Himmelfarb, N. Bansal, S.-I. Lee, From local explanations to global understanding with explainable AI for trees, Nat Mach Intell 2 (2020) 56–67. https://doi.org/10.1038/s42256-019-0138-9.

[35] H. Dey, W. Shao, H. Moradkhani, B.D. Keim, B.G. Peter, Urban flood susceptibility mapping using frequency ratio and multiple decision tree-based machine learning models, Nat Hazards 120 (2024) 10365–10393. https://doi.org/10.1007/s11069-024-06609-x.
[36] K. Magdiev, D. Fazilova, A. Kazakov, GIS-based Ecological Vulnerability Assessment in a Mountainous Region: the Charvak Reservoir, Uzbekistan, For. Geo. 40 (2026) 57–72. https://doi.org/10.23917/forgeo.13377.
[37] S. Kumar, B.R. Parida, Hydroponic farming hotspot analysis using the Getis–Ord Gi* statistic and high-resolution satellite data of Majuli Island, India, Remote Sensing Letters 12 (2021) 408–418. https://doi.org/10.1080/2150704X.2021.1895446.
[38] K. Khosravi, H. Shahabi, B.T. Pham, J. Adamowski, A. Shirzadi, B. Pradhan, I. Prakash, A comparative assessment of flood susceptibility modeling using multi-criteria decision-making analysis and machine learning methods, J. Hydrol. 573 (2019) 311–323. https://doi.org/10.1016/j.jhydrol.2019.03.073.
[39] E. Yildirim, I. Demir, Agricultural flood vulnerability assessment and risk quantification in Iowa, Science of The Total Environment 826 (2022) 154165. https://doi.org/10.1016/j.scitotenv.2022.154165.

Supplementary Material for

Prioritizing Agricultural Flood Mitigation: A GeoAI-Driven Assessment of Susceptibility, Crop Exposure, and Socioeconomic Vulnerability

Mirza Md Tasnim Mukarram[1,2], Mirza Waleed[3*], Quazi Umme Rukiya[1], Marc Linderman[1], Ibrahim Demir[4,5]

[1] School of Earth, Environment and Sustainability, University of Iowa, Iowa City, IA 52242, USA

[2] Department of Computer Science, University of Iowa, Iowa City, IA 52242, USA

[3] Department of Geography, Hong Kong Baptist University, Hong Kong Special Administration Region of China

[4] River-Coastal Science and Engineering, Tulane University, New Orleans, LA, USA

[5] ByWater Institute, Tulane University, New Orleans, LA, USA

*** Corresponding Author Email (WALEED M.):** waleedgeo@outlook.com

Corresponding Author Address: Office AAB1228, Academic and Administration Building, Hong Kong Baptist University, Hong Kong Special Administration Region of China

Table S3 Comparative performance of gradient boosting models for flood susceptibility mapping

Model	Accuracy	Precision	Recall	F1-Score	ROC-AUC (10-fold CV)
LightGBM	0.88	0.88	0.87	0.90	0.95 ± 0.00
XGBoost	0.87	0.87	0.86	0.89	0.94 ± 0.00
HistGBM	0.86	0.86	0.85	0.88	0.93 ± 0.01

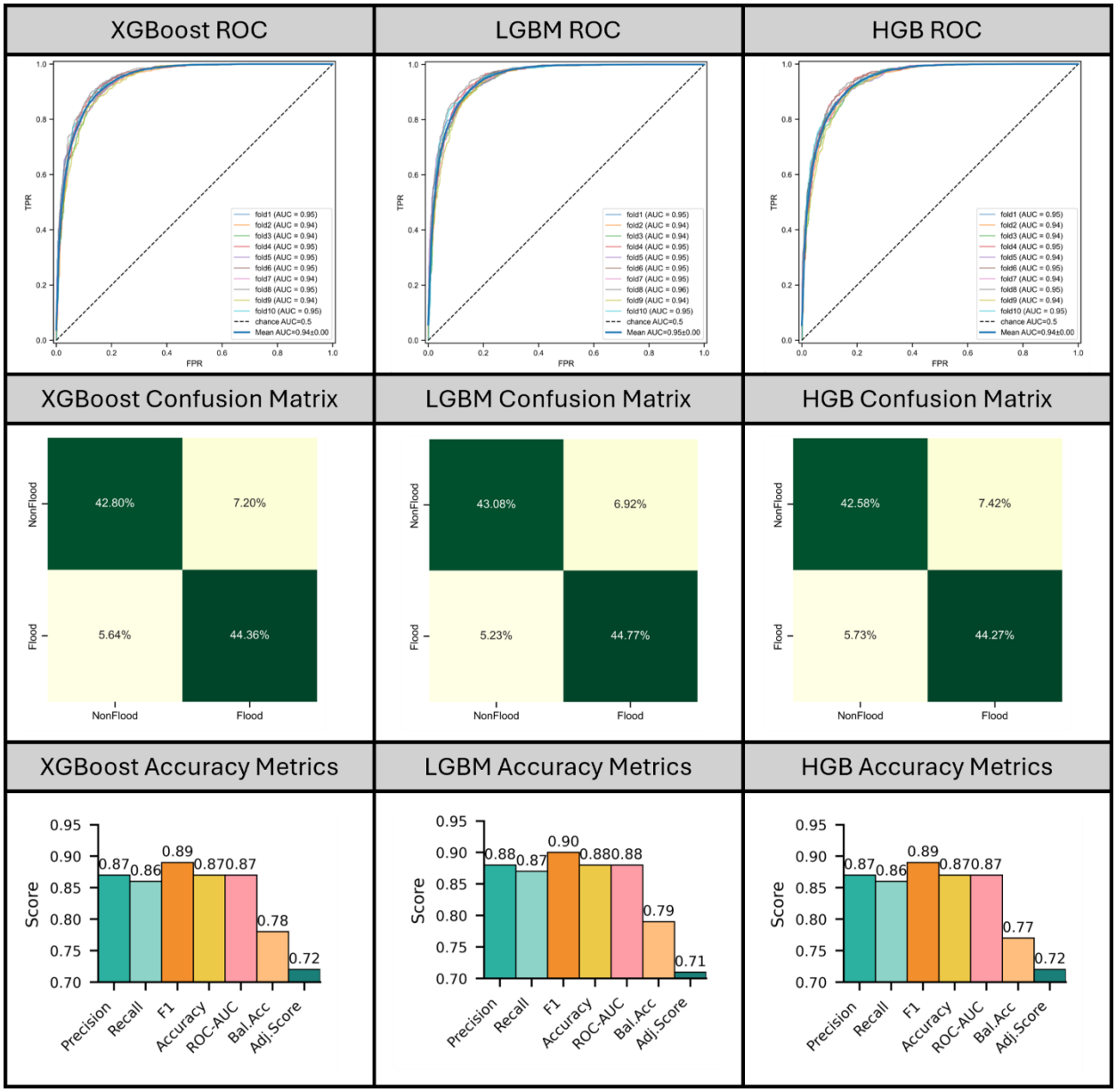

Figure S10 Performance evaluation of XGBoost, LightGBM, and HistGBM: ROC curves with AUC values; confusion matrices; comparative accuracy metrics.

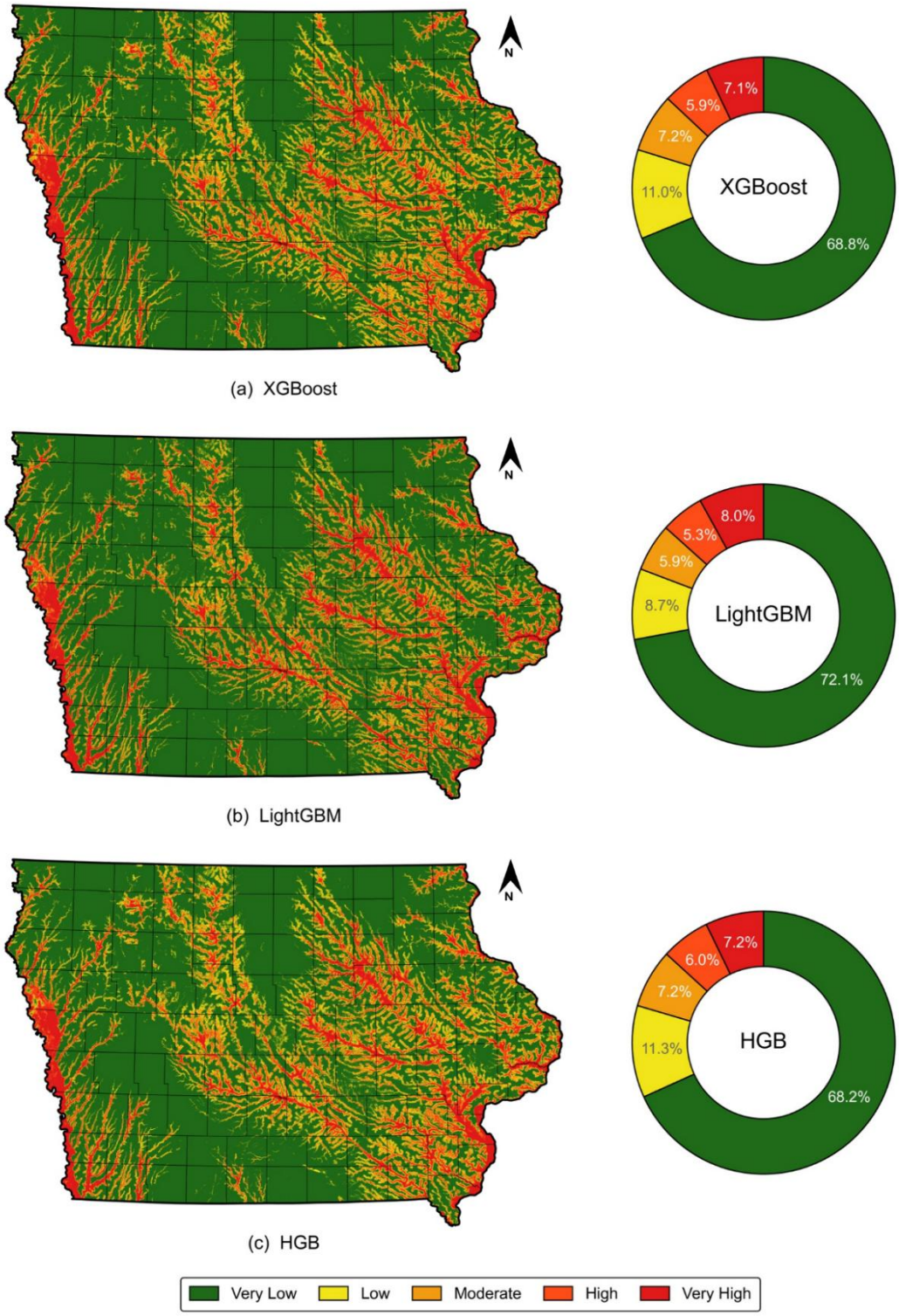

Figure S11 Flood susceptibility maps at 30 m resolution for Iowa: (a) XGBoost (High+Very High = 13.0%); (b) LightGBM (13.3%); (c) HistGBM (13.2%).

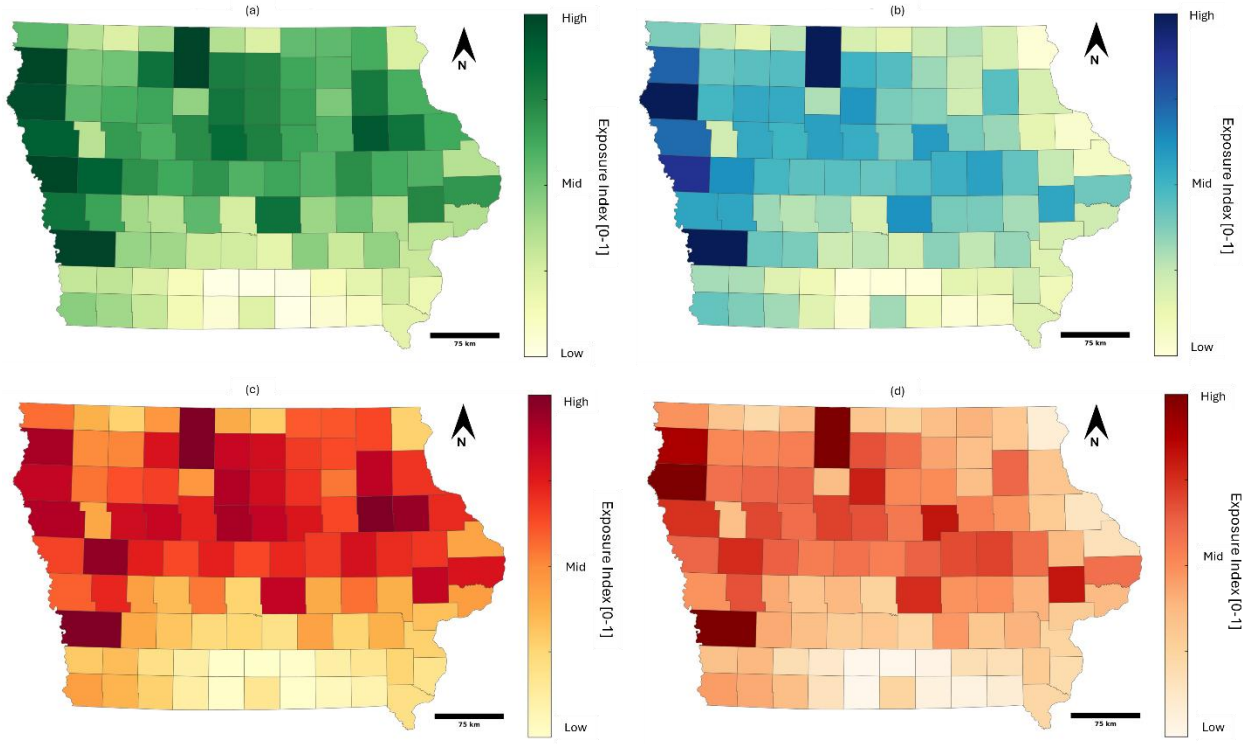

Figure S12 Agricultural exposure by county (USDA Census of Agriculture 2022): (a) corn harvested acreage; (b) soybean harvested acreage; (c) corn gross economic value; (d) soybean gross economic value. All surfaces normalized to [0–1] using 2nd–98th percentile clipping.

Table S4 Iowa agricultural exposure summary

Indicator	**Corn**	**Soybean**
Harvested Acreage	12,791,132 ac	9,580,405 ac
Top County (Acreage)	Kossuth (304,643 ac)	Pottawattamie (221,329 ac)
Price (USDA NASS 2022 Iowa avg.)	$4.50/bu	$11.50/bu
Gross Economic Value	$11.37B	$6.23B
Combined Total Gross Exposure	$17.60B	

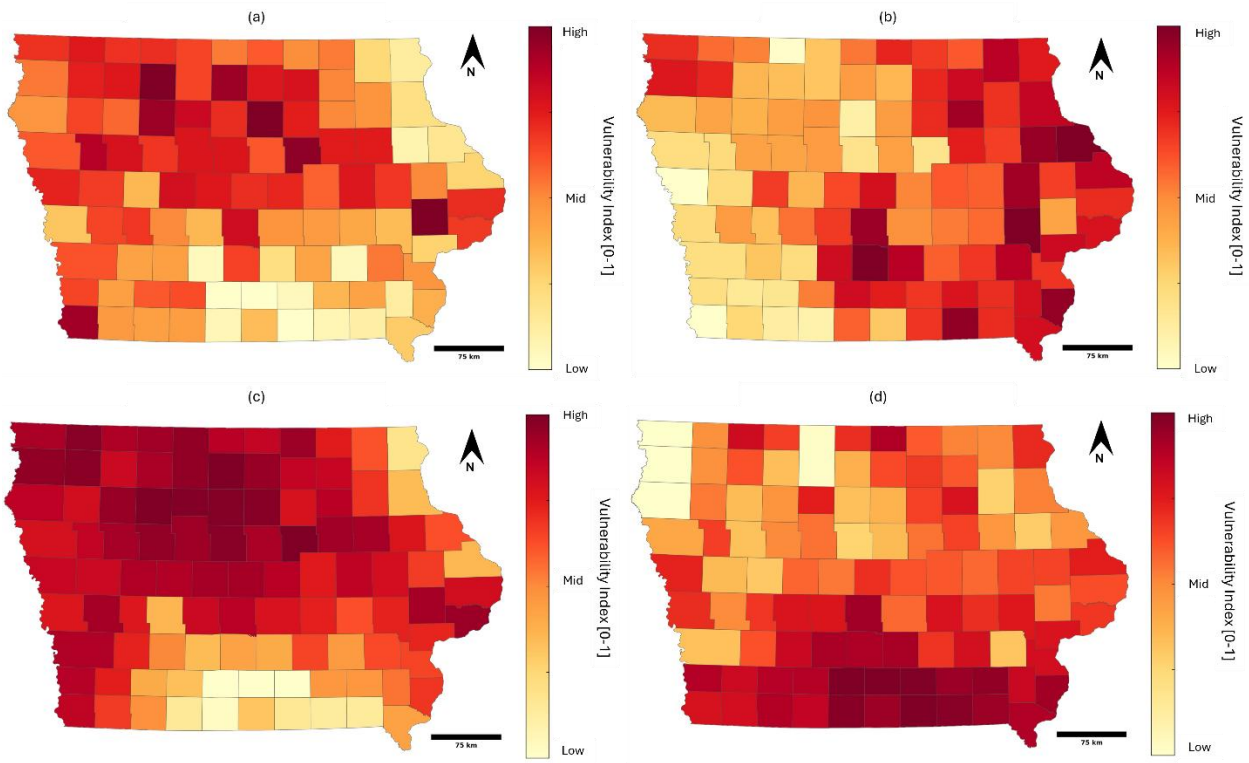

Figure S13 Socioeconomic vulnerability indicators: (a) tenant farming rate (mean = 63.4%, normalized mean = 0.536); (b) average farm size, inverted (mean = 358.3 ac, normalized mean = 0.552); (c) cropland intensity (mean = 77.2%, normalized mean = 0.717); (d) net farm income per operation, inverted (normalized mean = 0.610). All indicators normalized to [0–1].

Table S5 Iowa scenario-based expected annual agricultural flood loss summary.

Parameter	**Value**
Total Gross Revenue (VAR)	$17.36B
Flood Probability Proxy Range	0.050 – 0.350 (FSM-derived, scenario-based)
Insurance Coverage (Uniform)	78% (USDA RMA 2022 Iowa average)
Expected Corn Annual Loss	$353.8M/year
Expected Soybean Annual Loss	$173.9M/year
Total Expected Annual Loss	$527.7M/year
Loss as % of Gross Revenue	3.04%
Peak County: Monona	$19.9M/year (flood prob. proxy = 0.278)
#2 Pottawattamie / #3 Harrison	$13.2M / $12.4M per year

Table S6 County risk typology classification and policy implications

Priority Class	**Counties**	**Risk/Loss Profile**	**Policy Implication**
Priority 1	48	High Risk + High Loss	Highest urgency: targeted insurance reform and adaptation investment

Priority 2	2	High Risk + Low Loss	Structural vulnerability; monitoring and pre-positioned resources
Priority 3	2	Low Risk + High Loss	Exposure-driven; review insurance coverage adequacy
Priority 4	47	Low Risk + Low Loss	Lower urgency; maintain baseline monitoring

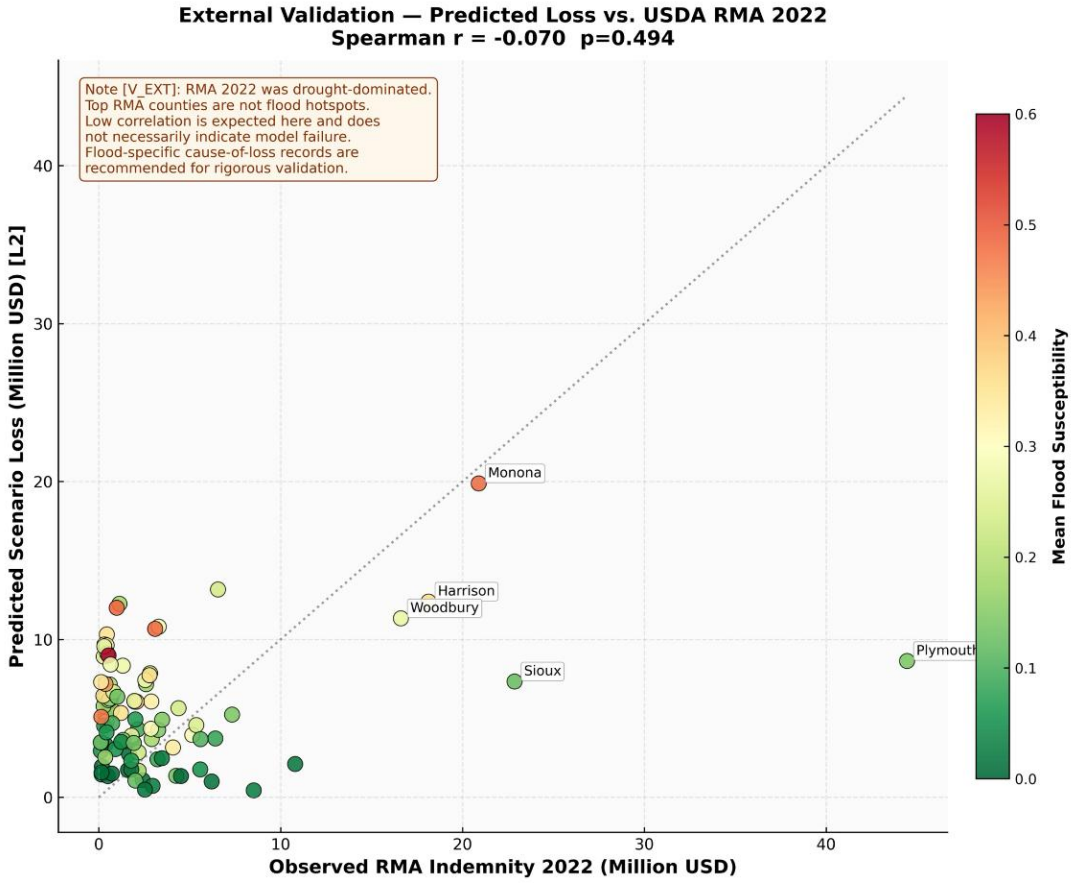

Figure S14 External validation: predicted county-level scenario-based loss vs. USDA RMA 2022 all-peril corn-soybean indemnity payments (Iowa total: $311.7M). Spearman $r_s = -0.070$, $p = 0.494$. Note: 2022 RMA was drought-dominated; low correlation is expected given the structural mismatch between the two datasets.